Elsevier Editorial System(tm) for Sedimentary Geology

Manuscript Draft

Manuscript Number:

Title: Sedimentary architecture and depositional controls of a Pliocene river-dominated delta in the semi-isolated Dacian Basin

Article Type: Research Paper

Keywords: Paratethys; Carpathian foredeep; isolated basin; river-dominated delta; regressive parasequences; autogenic forcing, flooding surfaces

Corresponding Author: Miss Elisabeth Louise Jorissen, MSc, IR

Corresponding Author's Institution: Utrecht University

First Author: Elisabeth Louise Jorissen, MSc, IR

Order of Authors: Elisabeth Louise Jorissen, MSc, IR; Arjan de Leeuw, Dr.; Christiaan G.C. van Baak, Dr.; Oleg Mandic, Dr.; Marius Stoica, Prof.; Hemmo A Abels, Dr.; Wout Krijgsman, Prof.

Abstract: Sedimentological facies models for (semi-)isolated basins are less well developed than those for marine environments, but are critical for our understanding of both present-day and ancient sediment records in restricted depositional environments.
Our proposed facies model considers an 835m-thick sedimentary succession, accumulated in a semi-isolated brackish embayment of the mid-Pliocene Black Sea. We investigated the sedimentary processes and depositional controls responsible for the sedimentary architecture of a delta flowing into this semi-isolated basin. The deltaic progradation caused a regressing from distal shelf deposits with brackish-water faunas to proximal fluvial deposits with fresh-water faunas. The observed facies architecture is typical for a river-dominated delta. The deltaic progradation into a restricted depositional environment probably resulted in the river domination and in a near-absence of sediment redistribution by wave- or tidal processes. The basin was filled with brackish-water, enhancing frequent hyperpycnal plumes, ichnofossils activity, enrichment in organic material and the preservation of in situ brackish- and fresh-water faunas. The delta prograded into a shallow basin on a low-gradient slope, creating thin sharp based sand bodies in numerous thin parasequences, due to a multiplication of the terminal distributary channels, covering a wide depositional area.
The parasequences are bounded by reddish oxidized shell-rich indurated flooding surfaces, formed by sediment starvation on the top of the abandoned delta lobes, due to frequent delta-lobe switching. As a result, a succession of 64 parasequences occurs, with a thinning from 15 to 95m from towards the top of the section. These high-frequency parasequences combine into nine low-order regressive sequences of around 83m and into three high-order regressive sequences of around 300m. A robust magnetostratigraphic time frame permitted to compare the observed sedimentary cyclicity with the amplitude and the frequency of various climatic cycles including astronomical forcing. Our results show that the frequencies of the parasequences and sequences are not in line with any

Milankovitch climatic cycle. This suggests that astronomical climate forcing didn't influence autogenic delta-lobe switching.

Suggested Reviewers: Cornel Olariu
University of Texas at Austin
cornelo@jsg.utexas.edu
Cornel Olariu has been working on several delta flowing into semi-isolated basins, including the Danube Delta.

Orsolya Sztanó
Eötvös Loránd University
sztano.orsolya@gmail.com
Orsolya Sztanó has been working on several delta flowing into Paratethyan semi-isolated basins, such as the Panonian Basin formed in the eastern foreland basin of the Carpathians.

John Howell
Kings College
john.howell@abdn.ac.uk
John Howell has been studied onshore analogue data to better understand the subsurface reservoir.

Gary Hampson
Imperial College London
g.j.hampson@imperial.ac.uk
Gary Hampson has been working on controls on deltaic architecture in the region of Utah, presenting similarities with our studied semi-isolated basin.

Miquel Poyatos
University of Oslo
m.p.more@geo.uio.no
Miquel Poyatos has been working on processes and controlling factors of sediment dispersal from river-mouth to base-of-slope settings.

Mathieu Schuster
Université de Strasbourg
mschuster@unistra.fr
Mathieu Schuster has been working on continental and coastal sedimentology in lacustrine environments.

Dear Editor,

Hereby I would like to submit our manuscript entitled "Sedimentary architecture and depositional controls of a Pliocene river-dominated delta in the semi-isolated Dacian Basin" by Elisabeth L. Jorissen, Arjan de Leeuw, Christiaan G.C. van Baak, Oleg Mandic, Marius Stoica, Hemmo A. Abels and Wout Krijgsman, for publication in Sedimentary Geology.

In this work, we investigate how the sedimentary architecture of a delta flowing into a semi-isolated basin differs from deltas prograding into the open ocean. We aim to better understand the sedimentary processes and controlling factors responsible for sediment deposition in restricted basins.

We studied an 835m-thick, continuous and very well exposed Pliocene section in the Dacian Basin, a former embayment of the Black Sea. The quality of the section allows establishing a detailed sedimentological and sequence-stratigraphic framework of a river-dominated delta prograding in a semi-isolated basin. The section's high-resolution magnetostratigraphic record moreover provides direct insight into the timescales at which environmental changes have taken place. This study may form a good, time-constrained analogue for more poorly exposed or subsurface enclosed deltas throughout the world.

Based on detailed field observations along the entire section, we identified thirteen lithofacies, grouped into five main facies associations. The facies model highlights a deltaic progradation from pro-delta clays to delta-top fluvial sands. The deltaic architecture displays a rhythmic succession of 64 parasequences with an average thickness of 13.5m, grouped into nine low-order regressive sequences of around 100m and into three high-order regressive sequences of around 300m. Particularly important is that the chronostratigraphy of the section indicates that these rhythmic environmental changes do not follow Milankovitch periodicities and are therefore likely autocyclic. The collected dataset constitutes a solid foundation to discuss the depositional controls acting on deltas prograding into restricted basins.

This manuscript has not been previously published and has not been submitted elsewhere for publication. Please don't hesitate to contact me if you require further information.

Thank you for considering my application, and I look forward to hear back from you.

Yours sincerely,

Elisabeth L. Jorissen

Highlights (for review)

- Facies model for river-dominated deltas prograding into (semi-)isolated basins different from open-marine deltas.
- Numerous thin parasequences due to frequent autogenic delta-lobes switching, covering a wide distributary area.
- Parasequences overlain by condensed, shell-rich and glauconite-rich flooding surfaces.
- Rhythmic environmental governed by autogenic deltaic processes without any astronomical climate forcing.
- Pliocene Paratethyian Dacian Basin formed a semi-isolated, brackish, shallow basin with a low-angle slope.

Sedimentary architecture and depositional controls of a Pliocene river-dominated delta in the semi-isolated Dacian Basin

Elisabeth L. Jorissen [a]*, Arjan de Leeuw [b,c], Christiaan G.C. van Baak [a,c], Oleg Mandic [d], Marius Stoica [e], Hemmo A. Abels [f], Wout Krijgsman [a]

a Palaeomagnetic Laboratory 'Fort Hoofddijk', Faculty of Geosciences, Utrecht University, Budapestlaan 17, 3584 CD, Utrecht, The Netherlands, e.l.jorissen@uu.nl; W.Krijgsman@uu.nl

b Université Grenoble Alpes, Institut des Sciences de la Terre, 38000 Grenoble, France, arjan.de-leeuw@univ-grenoble-alpes.fr

c CASP, West Building, Madingley Rise, Madingley Road, Cambridge, CB3 0UD, United Kingdom, C.G.C.vanBaak@uu.nl

d Geological-palaeontological Department, Natural History Museum Vienna, Burgring 7, 1010 Vienna, Austria, oleg.mandic@NHM-WIEN.AC.AT

e Department of Palaeontology, Faculty of Geology and Geophysics, University of Bucharest, Bălcescu Bd. 1, 010041, Romania, marius.stoica@g.unibuc.ro

f Department of Geosciences and Engineering, Delft University of Technology, Stevinweg 1, 2628 CN, Delft, The Netherlands, H.A.Abels@tudelft.nl

Abstract

Sedimentological facies models for (semi-)isolated basins are less well developed than those for marine environments, but are critical for our understanding of both present-day and ancient sediment records in restricted depositional environments.

Our proposed facies model considers an 835m-thick sedimentary succession, accumulated in a semi-isolated brackish embayment of the mid-Pliocene Black Sea. We investigated the sedimentary processes and depositional controls responsible for the sedimentary architecture of a delta flowing into this semi-isolated basin. The deltaic progradation caused a regressing from distal shelf deposits with brackish-water faunas to proximal fluvial deposits with fresh-water faunas. The observed facies architecture is typical for a river-dominated delta. The deltaic progradation into a restricted depositional environment probably resulted in the river domination and in a near-absence of sediment redistribution by wave- or tidal processes. The basin was filled with brackish-water, enhancing frequent hyperpycnal plumes, ichnofossils activity, enrichment in organic material and the preservation of *in situ* brackish- and fresh-water faunas. The delta prograded into a shallow basin on a low-gradient slope, creating thin sharp based sand bodies in numerous thin parasequences, due to a multiplication of the terminal distributary channels, covering a wide depositional area.

The parasequences are bounded by reddish oxidized shell-rich indurated flooding surfaces, formed by sediment starvation on the top of the abandoned delta lobes, due to frequent delta-lobe switching. As a result, a succession of 64 parasequences occurs, with a thinning from 15 to 95m from towards the top of the section. These high-frequency parasequences combine into nine low-order regressive sequences of around 83m and into three high-order regressive sequences of around 300m. A robust

magnetostratigraphic time frame permitted to compare the observed sedimentary cyclicity with the amplitude and the frequency of various climatic cycles including astronomical forcing. Our results show that the frequencies of the parasequences and sequences are not in line with any Milankovitch climatic cycle. This suggests that astronomical climate forcing didn't influence autogenic delta-lobe switching.

Key-words: Paratethys, *Carpathian foredeep*, *isolated basin*, *river-dominated delta*, *regressive parasequences*, *autogenic forcing*, *flooding surface*

1 Introduction

Ancient, long-lived lakes and semi-isolated basins provide valuable environmental, climatic and biological archives. Various deep-drilling projects in long-lived lakes across the globe (Cohen, 2012) and in semi-isolated basins, such as the Black Sea (Ross, 1978), have significantly enhanced our understanding of their evolution. However, the data integration from cores and outcrops is commonly challenging (Wilke et al., 2016). Outcrops of deltaic deposits that accumulated in lakes and semi-isolated basins are relatively rare, but can provide wider spatial and temporal insights into sedimentary facies, fauna distributions and climate forcing.

Deltaic facies models for (semi-)closed basins are less well developed than those for marine environments (Andrews et al.,

2016; Nutz et al., 2017). Deltas flowing into lakes or restricted basins form complex systems that exhibit great varieties of environments and faunal habitats (Panin and Jipa, 2002; Barth et al., 2014). We can, however, expect that these deltas record some specific facies characteristics related to their unusual settings. In these restricted basins, deltas prograde into low energy environments, which generally lack tidal influence and often show reduced wave interference. Their resulting internal architecture is therefore usually river dominated (Vakarcs et al., 1994; Kroonenberg et al., 2005; Olariu and Bhattacharya, 2006; e.g. Fielding, 2010; Hampson et al., 2011).

Restricted basins form unusual depositional environments, where depositional forcing mechanisms often differ from the open ocean. These basins are generally rapidly filled (Magyar et al., 2013), since their development is mostly controlled by sediment supply, water supply and water depth (Bohacs et al., 2003). The position and relative height of sills or spill points exert an important control on facies architecture in (semi-)isolated basins (Bohacs et al., 2003; Leever et al., 2010; Yanina, 2014; Fongngern et al., 2016). As soon as the basins are filled, the accommodation space becomes limited (Bohacs et al., 2000, 2003) and water and later sediments start to spill out into adjacent basins (Leever et al., 2011; Ter Borgh et al., 2014). If the tectonic subsidence is fast enough to maintain high sedimentation rates, sediment overspill may never occur, and the system remains balanced. The isolated nature of these balanced system often enhance their sensitivity to forcing factors (Müller

et al., 2001; Abels et al., 2009, 2010; Leroy et al., 2014; Litt and Anselmetti, 2014; Wagner et al., 2014; Constantinescu et al., 2015; Neubauer et al., 2016).

Semi-isolated basins are typically brackish- to fresh-water environments, due to their restricted connectivity with the marine realm. Lowered salinities usually lead to the development of faunas endemic to the basins (e.g. Jones and Simmons, 1996; Rögl, 1998; Wesselingh et al., 2006). Particular species can proliferate during periods when conditions throughout the basin are optimal for their development. However, their preferred habitat may become limited to certain refuges when the conditions in the basin are adverse (Nevesskaya et al., 2009; Popa et al., 2009). Palaeogeographical reconstructions are therefore extremely challenging in these settings. It is in this regard vital to integrate sedimentological and biological observations over a wide range of timescales and environmental settings (Wilke et al., 2016). This is also beneficial for the development of sedimentary facies models and has the potential to change the understanding of the role of delta progradation in shaping the stratigraphy of enclosed basins (Magyar and Geary, 2012).

In this paper, we investigate the mid-Pliocene sedimentary architecture of a river-dominated delta entering the semi-isolated Dacian Basin in Romania. The Dacian Basin formed a brackish embayment of the ancient Black Sea. Sediments that accumulated along the northern margin of the Dacian Basin during the Late Miocene and Pliocene have subsequently been

exhumed due to thrusting in the SE Carpathians (Matenco and Bertotti, 2000). As a result, a thick and continuous section of fossil-rich sediments crops out along the Slănicul de Buzău River (Andreescu et al., 2011; Van Baak et al., 2015). The quality and continuity of the exposure allows a detailed sedimentological and sequence-stratigraphic framework to be established. When combined with shifts in the associated mollusc and ostracod faunas, these can be used to investigate the drivers of internal deltaic architecture. Moreover, because of available magnetostratigraphic time constraints (Van Baak et al., 2015), the impact of autogenic versus allogenic factors on the deltaic sedimentary architecture can be discussed.

Facies models developed in this paper may form good analogues for more poorly exposed or subsurface (semi-)isolated basin deltaic successions. More specifically, it provides valuable sedimentological insights for all deltas flowing into ancient Paratethys basins (e.g. the Volga, Don, Dnieper and Amu Darya deltas).

2 Geological background

The Paratethys Sea formed one of the largest intercontinental seas that ever existed (Rögl, 1998; Popov et al., 2006). During the Oligocene, convergence between Africa and Eurasia generated a topographical barrier, which isolated the Paratethys Sea from the Tethys Ocean (Rögl, 1998; Allen and Armstrong, 2008; Schmid et al., 2008). As a result, the Paratethys Sea became a large brackish, semi-isolated basin. Miocene and

Oligocene tectonic activity produced numerous mountain belts (Vincent et al., 2007, 2016; Schmid et al., 2008) and further fragmented the Paratethys Sea into several brackish- to fresh-water semi-isolated basins (Popov et al., 2006). From west to east, the four major ones are the Pannonian, Dacian, Euxinian (Black Sea) and Caspian basins (Fig. 1a). Deposition in each basin was controlled by regional geodynamic, climatic and palaeoenvironmental factors. Their chronostratigraphy is therefore based on regional stages (e.g. Piller et al., 2007) (Fig. 2a). This paper focuses on the Dacian Basin, which formed an embayment of the Black Sea (Fig. 1b). FIGURE 1

The Dacian Basin represents the Late Miocene to present-day foreland basin of the Eastern and Southern Carpathians (Matenco and Bertotti, 2000; Cloetingh et al., 2004; Panaiotu et al., 2007; Jipa, 2015). The Carpathians were created during the progressive subduction of a slab under the Tisza-Dacian and Alcapa micro-continents (Bertotti et al., 2003; Schmid et al., 2008; Matenco et al., 2010). This slab detached progressively with a tear migrating from NW to SE along the Carpathian arc (Wortel and Spakman, 2000). As a result of the focussed downward pull of the partially detached slab, in combination with foreland flexure due to orogenic loading, a particularly deep depocentre formed in front of the Southeast Carpathians (Bertotti et al., 2003; Tărăpoancă et al., 2003).

The depression was progressively filled with the erosion products of the uplifted mountains (Jipa, 1997; Sanders et al., 1999; Tărăpoancă et al., 2003; Panaiotu et al., 2007). Deep open-

water deposits with brackish-water faunas, which accumulated in the basin during the Late Miocene-Early Pliocene (Pontian regional stage - Stoica et al., 2013), were gradually replaced by delta-top deposits with fresh-water faunas towards the Late Pliocene (Romanian regional stage - Van Baak et al., 2015). This transition of depositional environments occurred during the intermediate regional Dacian stage, which lasted from 4.8 to 4.2 Ma (reviewed by Vasiliev et al., 2005; Van Baak et al., 2015) (Fig. 2a). At that time, sediments shed from the Southern Carpathians mainly accumulated in the western Dacian Basin (Jipa and Olariu, 2009; Jipa et al., 2011; Ter Borgh et al., 2014; Fongngern et al., 2017 accepted), whereas a major delta prograded along the Eastern Carpathians towards the northeastern margin of the Dacian Basin (Jipa, 1997; Jipa and Olariu, 2009; Fongngern et al., 2016; Matoshko et al., 2016) (Fig. 1b). Palaeogeographic and provenance data indicate that the basin was eventually entirely filled during the Late Pliocene to Early Pleistocene (Jipa and Olariu, 2009; De Leeuw et al., 2017 accepted; Olariu et al., 2017 accepted).

Post-collisional shortening affected the Carpathian Foredeep during the Quaternary (Necea et al., 2005; Leever et al., 2006; Maynard et al., 2012). Faulting and large-scale folding of the foreland infill occurred in the Slănicul de Buzău area (Fig. 2b).

FIGURE 2

3 The Slănicul de Buzău section

The investigated section crops out along the Slănicul de Buzău River, which has incised the folded foreland deposits (Fig. 2b). A composite section along various parts of the river exposes a 6.4 km thick stratigraphic succession of Late Miocene to Pleistocene sediments (Snel et al., 2006; Andreescu et al., 2011; Van Baak et al., 2015) (Fig. 2c). Our study focuses on the part of the section corresponding to the mid-Pliocene Dacian regional stage (Fig. 2a). Sediments attributed to this regional stage crop out at multiple points along the valley. The record we study extends from 45.440861°N, 26.743914°E to 45.452928°N, 26.745603°E. A good age model exists for this part of the valley (Van Baak et al. 2015). Magnetostratigraphic studies show that this section contains two normal magnetozones, interpreted as the Nunivak (C3n.2n: 4.631-4.493Ma) and the Cochiti (C3n.1n: 4.300-4.187Ma) chrons (age from Gradstein et al., 2012; Van Baak et al., 2015). The total studied section has an age between 4.7 Ma and 4.15 Ma. These age constraints are in line with studies of the Dacian regional stage at other locations in the Dacian Basin (e.g. Vasiliev et al., 2004).

In the Slănicul de Buzău section, the Dacian stage is 835m-thick, as measured in the field and checked by GPS measurements. In our section, relatively deep open-water clays are repetitively interrupted by shallower fluvial sands (Fig. 3a). The sandy layers become gradually more frequent towards the top. Throughout the Dacian stage, most of the sandy layers are topped by oxidized shell-rich layers. FIGURE 3

4 Methods

4.1 Biostratigraphic analyses

The studied section contains very rich mollusc and ostracod faunas, which were studied from 58 samples. Sample preparation for molluscs was performed at the Natural History Museum in Vienna and included mechanical cleaning using pneumatic micro-chisels, as well as washing and sieving over a 1 mm mesh. The general preservation of the shells was moderate to poor. Shells were finely cracked due to secondary gypsum mineralisation and carbonate crystal growth. Nevertheless, 1817 fossil specimens were analysed. The taxonomic identifications follow Wenz (1942) and Marinescu & Papaianopol (1995). Taxonomic revision incorporates results by Nevesskaya et al. (1997, 2001, 2013) and Neubauer et al. (2014).

Sample preparation for ostracods was carried out at the Department of Palaeontology at the University of Bucharest. Samples of 500-1000g were dried to remove interstitial water from the sediments. Dry samples were subsequently boiled for 30-60 minutes with a sodium carbonate solution for better disaggregation. The samples were then washed through several sieves of 63–500µm. The residues were analysed under a ZEISS–Stemi SV11 microscope and pictures of micro-faunas were taken with a NIKON digital camera. The general preservation of the ostracods was moderate to poor. Ostracods are fragmented due to strong diagenesis. The taxonomic identifications follow Hanganu (1976, 1985), Hanganu & Papaianopol (1977), Olteanu (1995) and Stancheva (1990).

4.2 Sedimentological model

The studied section had previously been logged at a meter-scale (Van Baak et al., 2015). This general log missed a 40m interval in the middle part of the section, which is now included in our renewed analysis (Fig. 3a). Some parts of the section are described at a centimeter-scale, in order to distinguish characteristic facies associations and to perform a detailed palaeoenvironmental reconstruction. Variations in lithology, grain size and sedimentary structures were recorded in the field. Sediment colors of fresh rocks were described using Munsell Soil Color Charts. Particular attention was paid to sedimentary structures, such as graded bedding, laminations, cross-stratification or ichnofossils. Sedimentological samples were collected for sedimentological and petrographic optical microscopic descriptions. Thin-sections of 30µm-thick were made perpendicular to the sedimentary structures for petrographic descriptions.

The detailed sedimentological observation allowed several facies associations to be established, each of them related to a specific depositional environment. A facies association depth ranking scale was constructed by attributing a number from 0 to 9 to facies associations, with for arbitrary reasons 0 being the deepest and 9 the shallowest depositional environment (Tab. 1). This facies association depth ranking scale permits the reconstruction of a relative water-level curve and the identification of parasequences, including superposed lower- and higher-order sequences. TABLE 1

4.3 Palaeocurrent determination

In total, 41 palaeocurrent directions were measured on 3D cross-beds. In the pro-delta deposits, the palaeocurrent directions were measured on trough-cross stratifications present in the lenticular-bedding. In the delta-front deposits, they represent trough cross-stratification, sigmoidal cross-stratification or climbing ripples. Finally, in delta-top deposits they additionally include low-angle cross-stratification and asymmetrical current ripples.

To correct palaeocurrent directions, we removed any tectonically-induced vertical-axis rotations with the help of the available palaeomagnetic dataset. Our bedding tilt measurements indicate the section is located on top of a plunging anticline with a fold axis of 31° azimuth and 19° plunge (Fig. 4). This requires a more complicated procedure of first deplunging the fold axis, followed by a second step of correcting for the true vertical axis rotation.

To correct for the plunging fold axis, all obtained palaeomagnetic directions, bedding planes and their poles were plotted in a stereographic projection using the Stereonet 9 software (Allmendinger et al., 2011; Cardozo and Allmendinger, 2013). Bedding planes and palaeomagnetic directions were subsequently rotated 19° around a rotation axis with a 121° azimuth and 0° plunge to restore the fold axis to horizontal (Fig. 4). The corrected palaeomagnetic directions were then entered as pre-tilt directions in the statistics portal of palaeomagnetism.org (Koymans et al., 2016), together with their

associated plunge-corrected bedding planes. Regular tilt-correction on the basis of these bedding planes, i.e. the second step of unfolding, was now applied to place the palaeomagnetic directions in their correct tectonic reference frame. Subsequent regular statistical analysis revealed a plunge-corrected anticline with a mean direction of 171°. This implies a 9° counter clockwise horizontal plane rotation of the section along the Slănicul de Buzău River, due to the deformation of the Carpathian Bend zone. These results are in line with the previously determined 14° rotation (Slănicul site of Dupont-Nivet et al., 2005; Vasiliev et al., 2009; Van Baak et al., 2015).

Once the palaeocurrent directions were corrected using the same principle, their statistical distribution was calculated for 12 sectors of 30° and plotted on rose diagrams with a maximum representability of 50% (Fig. 12). Palaeocurrent directions were plotted on different rose diagrams, both according to the overall flow direction along the section, as well as in their respective depositional environments. FIGURE 4

4.4 Cyclicity analysis

An age model was constructed using the existing well-constrained magnetostratigraphic timescale of the studied section. For each chron interval, the sedimentation rate was calculated in order to evaluate the variations through time of sediment input into the basin.

A cyclostratigraphical analysis was performed on the frequencies of the parasequences, low- and high-order sequences, to evaluate potential climatic forcing on the

sedimentation. Blackman-Tuckey power spectra were generated using standard settings on an equally-spaced data series in the Analyseries 2.0.4b program. Bandpass filters were generated in the same program using lows besides power peaks at 90% confidence levels. We then selected the 50-138m, 64-111m, 25-37m and 13.6-25m filters. These filters were then plotted against the facies rank data and the astronomical target curves.

5 Results

5.1 Bio-stratigraphic results

The semi-isolated Paratethyan basins registered episodic periods of connectivity and disconnectivity though time. Due to restricted water exchange between the basins, endemic mollusc and ostracod faunas developed in these brackish- to fresh-water environments (Marinescu, 1978; Stoica et al., 2013). Working in these atypical environmental conditions introduces a certain ambiguity between palaeontological and sedimentological terminology (Matoshko et al., 2016). Here, the terms 'brackish-water' and 'fresh-water' are used to specify the basin's salinity on the basis of palaeontological indicators. The term 'open water' is on the contrary used in a sedimentological context in order to describe offshore to shoreface depositional environments.

Along the Dacian part of the Slănicul de Buzău section, 47 mollusc species have been identified, comprising 33 bivalve and 14 gastropod species (Tab. 2 & Fig. 5). Bivalves account for 70% of the 1817 identified individuals, and are dominated by lymnocardiinae cardiids. They preferentially live in brackish-

375 water basins (Nevesskaya et al., 2001) and represent low energy
376 depositional environments when they are *in situ*. In contrast, the
377 presence of *in situ* unionids (2 species) and viviparids (2 species)
378 (Mandic et al., 2015 and reference therein) indicates fresh-water
379 conditions in delta-top types of environments. However, both
380 species groups are often transported postmortem, either towards
381 the deeper parts of the basin by storm or gravity currents, or to
382 the shallower parts of the basin by current activity. More detailed
383 palaeoenvironmental descriptions using the fossils will follow in
384 the sections describing the different sedimentary facies (Section
385 5.2). TABLE 2/FIGURE 5
386 Fauna distributions allow identifying the boundaries
387 between the regional (sub)stages, in order to improve the time
388 frame of the studied section. Firstly, the boundary between the
389 older Pontian and the Dacian stages was recognized as being
390 transitional. We observe that many ostracod faunas present
391 during the Pontian stage gradually disappear and are replaced by
392 different species during the Dacian stage. Some ostracod species,
393 such as *Pontoniella, Bakunella, Tyrrhenocythere, Camptocypria,*
394 *Cytherissa* and *Caspiocypris*, which have their maximum
395 development within the Pontian stage, are still present during
396 the Dacian, but are less abundant. Likewise, some ostracod
397 species, which already appear in the Pontian, present their
398 maximum development during the Dacian. The changes in the
399 ostracod distribution at the Pontian/Dacian boundary seem to
400 have been the result of a water freshening. This aspect is marked
401 by the appearance of the fresher-water genus *Cyprideis* ex. gr.

torosa in the Dacian stage. The boundary between these two stages was dated at 4.8±0.1 Ma (Dupont-Nivet et al., 2005).

Secondly, the fauna distributional permitted to locate the boundary between the Lower/Upper Dacian regional substages (Tab. 2), as defined by Marinescu & Papaianopol (1995). The Lower Dacian index mollusc species *Pachydacna* (*Parapachydacna*) *serena* is present in the interval from 80 to 503m. This range coincides with the range of *Psilodon munieri*, present between 110m and 503m, which is also confined to the Lower Dacian substage. In this lowest part of the section, *Zamphiridacna orientalis* and *Viviparus argosiensis* show their topmost occurrences. Moreover, *Stylodacna heberti*, with a last occurrence at 621m, shows maximal abundance in the Lower Dacian. Furthermore, the Lower Dacian is marked by the important development of some characteristic ostracod species (Fig. 6 & Fig. 7). The fresh-water species *Cyprideis torosa*, appears during the Lower Dacian. Several species of candonidae are also present, such as *Candona neglecta, Caspicypris alta, Camptocypria balcanica* and *Pontoniella* ex. gr. *quadrata*. An important and somewhat a marker of Lower Dacian is *Scottia dacica.* This species is however very rare and badly preserved in our section. *Cytherissa boghatschovi* and *Amplocypris sp.* can also be considered as characteristic futures of the Lower Dacian ostracod assemblages. Additionally, we notice in this interval the presence of *Amnicythere multituberculata, Amnicythere andrusovi, Amnicythere ex. gr. cymbula, Loxoconcha schweyeri* and *Loxoconcha babazananica*. In contrast, the Upper Dacian index

mollusc species *Psilodon haueri* extends from 445m to 720m in our section (Tab. 2). The other Upper Dacian index fossil *Zamphiridacna zamphiri* occurs likewise between 561 and 815m. On the basis of these observations, the Lower/Upper Dacian substage boundary should be located between 445m and 503m.

FIGURE 6/ FIGURE 7

This boundary is confirmed by changes of ostracod assemblages in the Upper Dacian (Fig. 8 & Fig. 9). Ostracods faunas differ both qualitative and quantitative between these two substages. From a qualitative point of view, we observe that many Pontian species, which still survived during the Lower Dacian, completely disappeared or a very rare in the Upper Dacian. It is for example the case of *Bakunella dorsoarcuata* and many leptocytheridae and loxoconchidae species. Quantitatively, *Cyprideis* species is even more abundant in the Upper Dacian than in the Lower Dacian. This taxa is associated with *Cytherissa* spp., like *Cytherissa bogathschovi* or *Cytherissa lacustris*. They occur together with *Caspiocypris ornatus*, *Cyprinotus sp*, *Amplocypris* sp.. They are also associated with two cyprididae ostracods, known as *Scottia kempfi* and *Scottia bonnei* (Hanganu, 1976), possible direct descendants of the Lower Dacian species *Scottia dacica*. Species of *Camptocypria* genus, very common during the Lower Dacian, are now represented just by *Camptocypria balcanica*. From loxoconchidae, we now only identifie *Loxoconcha* ex. gr. *scheweri*. Furthermore, the Upper Dacian is marked by a decrease in abundance of *Pontoniella ex.*

gr. truncata, Ilyocyris bradyi, Ilyocypris gibba, Darwinulla stevensoni and *Cyclocypris laevis.*

Finally, the boundary between the Dacian and the younger Romanian stages could also be identified thanks to the mollusc distributional data (Tab. 2). The topmost Upper Dacian is marked by the presence of *Psilodon neumayri,* which is found up to the very top of the section, from 698m to 815m. More thorough fauna distribution analyses were previously realized at the boundary between these two regional stages, dated at 4.2±0.1 Ma (Van Baak et al., 2015). FIGURE 8/FIGURE 9

5.2 Sedimentary facies associations

The 835m-thick succession displays a generally regressive trend, superposed by a rhythmic alternation between more distal clays and more proximal sands (Fig. 3a). Our field observations and subsequent microscope descriptions were compared to well documented sedimentological classifications (Postma, 1990; Miall, 2006). This allowed us to distinguish thirteen lithofacies, formed by different sedimentary processes (Tab. 3). Stratigraphically-related lithofacies represent eight depositional facies, which were grouped into five main facies associations, each of them interpreted as related to a distinct depositional environment. TABLE 3

5.2.1 Pro-delta facies association

5.2.1.1 Description

The first facies association is generally 1 to 5m-thick. It consists of three types of dark-bluish-gray (GLEY2-4/5B) to bluish-gray (GLEY2-5/5B) mudstone that occur successively.

There are massive (labeled Fm), laminated (Fl) and lenticular (Fs) mudstones. Massive mudstones (Fm) occur at the base of the pro-delta facies association strata. These massive mudstones are 0.5 to 1m-thick, but sometimes are absent from this facies association. They display a dark-bluish-gray color (Fig. 10b). They may contain low numbers of well-preserved, *in situ*, brackish-water molluscs, such as *Euxinicardium olivetum, Pontalmyra tohanensis* or *Chartoconcha rumana* (Tab. 4 & Fig. 5, respectively 1, 5 and 10). Facies Fm is progressively replaced by 1 to 3m-thick, laminated gray mudstones (Fl). These mudstones have millimeter-scale planar laminations of silt (Fig. 10c). They may also contain centimeter-scale planar laminations of silt with millimeter-scale terrestrial organic material fragments. Upwards, the muddy succession may contain 0.5 to 1m-thick, gray mudstones with lenticular bedding (Fs). The lenticular bedding consists of 1 to 5cm isolated lenses made of silt to very-fine sand showing trough cross-stratification (Fig. 10d). The sandy layers are occasionally affected by convolute bedding of centimeter-scale. Throughout this facies association, the laminations and the lenses become thicker, more frequent, and composed of coarser sediments toward the top. The palaeocurrents measured in these deposits demonstrate a mean direction of 225° (n=17; Fig. 12a). They display a wide range of current directions from 180° to 270°.

These deposits occasionally show intercalations of centimeter-thick beds of gray sandstones (GLEY1-6/N). These sandstones Sfg are fine to medium-grained, well-sorted, and

structureless (Fig. 10e). Petrographic analysis shows highly-spherical and sub-angular quartz grains. Their bases form a wavy, sharp surface, highly perturbed by vertical burrows of 3 to 5cm wide and 5 to 15cm deep. The sandstones contain many abraded or broken, reworked, brackish- and fresh-water molluscs, such as different species of cardiids, unionids, dreissenids or viviparids. FIGURE 10/ FIGURE 11

5.2.1.2 Interpretation

This facies association is interpreted to represent a pro-delta environment because of the distal depositional setting and the evidence of distal fluvial input. The massive mudstones (Fm) highlight deposition out of suspension in open water. The progressive transition to millimeter-scale silty laminations (Fl) is related to large fluvial outflows, energetic enough to reach the distal part of the basin. The centimeter-scale, organic-rich, silty laminations could be related to hyperpycnal flows, associated with episodic larger river discharge events (Mulder et al., 2003; Bhattacharya and MacEachern, 2009; Lamb and Mohrig, 2009). Upwards, the gradual occurrence of silty lenticular bedding (Fs) is related to wave action and/or winnowing (De Raaf et al., 1977). The sandy beds comprising reworked, abraded and broken shells (Sfg) are thought to illustrate sporadic higher energetic depositional processes occurring in the muddy surrounding environment. These coarser structureless sediments were transported into the basin over long distances during intermittent sand influxes. As in previous studies (Starek et al.,

2010; Hampson et al., 2011), these sandstones are interpreted as storm deposits.

The coarsening character within this facies association illustrates an increase in the energy of the depositional process and is seen as a shallowing of the environment. Following earlier studies of similar muddy facies associations (Overeem et al., 2003; Olariu and Bhattacharya, 2006; Fielding, 2010), we propose that these sediments have been deposited in pro-deltas. The large range of palaeocurrent directions highlights the development of several delta-lobes, feeding a wide pro-delta region. TABLE 4

5.2.2 Distal delta-front facies association

5.2.2.1 Description

The second facies association shows a 0.5 to 5m-thick, regular alternation between centimeter- to decimeter-thick layers of mudstones and sandstones. The mudstones are blueish-gray (GLEY2-5/5B). They record millimeter- to centimeter-scale planar laminations of silts or very-fine sands (Fl), centimeter-scale planar laminations of silt or very-fine sand with millimeter-scale terrestrial organic material fragments and lenticular bedding made up of centimeter-scale lenses with trough cross-stratified silt to very-fine sand (Fs). They are intercalated with layers of grayish-brown sands (2.5Y-5/2). These sands are very-fine to fine-grained, moderately sorted, and contain low-spherical and sub-angular grains. The sandstones show three types of centimeter-scale cross-beddings. Facies Sr corresponds to 10 to 50cm-thick climbing ripples (Fig. 11b). Facies Ss displays

20 to 100cm-thick sigmoidal cross-stratification (Fig. 11c). Finally, facies St comprises 10 to 50cm-thick trough cross-stratification (Fig. 11d). The foresets of these cross-beddings are commonly draped by millimeter-scale laminae of terrestrial organic matter fragments. The sandstones frequently show convolute bedding of centimeter- to decimeter-scale. The sandy beds become thicker, more frequent, and are composed of coarser sediments toward the top of the facies association.

Like in the previous pro-delta facies association, the deposits are occasionally interupted by the same centimeter-thick beds of gray (GLEY1-6/N) structureless, medium-grained and well-sorted sandstones Sfg (Fig. 11e), with highly-spherical and sub-angular quartz grains. Their bases display the same wavy, sharp, highly bioturbated surface. Here as well, they contain many reworked, abraded and broken brackish- and fresh-water molluscs.

5.2.2.2 Interpretation

This facies association is interpreted as representing a distal delta-front environment more frequently influenced by fluvial input as the previous facies association. The mudstones were deposited out of suspension in open waters. The episodic intercalations of sandstones are related to increases of sand input coming from the distal margin of distributary channels. Once these sands reach the distal delta lobe, they record a relative deceleration and form centimeter- to decimeter-scale, migrating, sub-marine dunes comprising small-scale cross-bedding. The lenticular bedding (Fs) is related to wave action

589 and/or winnowing (De Raaf et al., 1977). The climbing ripples
590 may be related to rapid sedimentation rates and non-uniformity
591 flows, due to a loss of the sediment confinement or a decrease in
592 slope gradient (Jobe et al., 2012). The centimeter-scale, organic-
593 rich, silty laminations could be related to hyperpycnal flows,
594 occurring during episodic larger river discharge events (Mulder
595 et al., 2003; Bhattacharya and MacEachern, 2009; Lamb and
596 Mohrig, 2009). The convolute bedding could have been created
597 when the sandstones were rapidly deposited on the underlying
598 water-saturated mudstones, causing an expulsion of the fluids
599 contained in the mud (Oliveira et al., 2009). The shell-rich sandy
600 beds (Sfg) sporadically intercalated in this facies association
601 suggest, here as well, storm deposits (Starek et al., 2010;
602 Hampson et al., 2011).
603 This facies association, showing a coarsening up, displays an
604 increase in the energy of the depositional process and illustrates
605 a depositional environment gradually closer to the distributary
606 system. In line with previous studies on similar facies
607 associations (Fielding, 2010; Hampson et al., 2011), the
608 depositional setting was interpreted as a distal delta-front
609 environment.

610 ### 5.2.3 Proximal delta-front facies association

611 #### *5.2.3.1 Description*

612 The third facies association is marked by the lack of
613 mudstones. It is composed of 0.5 to 2m-thick, grayish-brown
614 (2.5Y-5/2), fine-grained sandstones. The sands are moderately
615 sorted, have low sphericality and are sub-angular. They form

decimeter-scale layers and comprise the same 3 types of cross-beddings, but at a decimeter-scale. Facies labeled Sr contain 10 to 50cm-thick sets of climbing ripples (Fig. 11b). Facies Ss displays 20 to 100cm-thick sigmoidal cross-stratification (Fig. 11c). Finally, facies St comprises 10 to 50cm-thick trough cross-stratification (Fig. 11d). The sedimentary structures are draped by millimeter-scale terrestrial organic material fragments. The palaeocurrent directions measured in this and the previous facies association demonstrate a mean direction of 180° (n=19; Fig. 12b), with a range from 90° to 330°. FIGURE 12

5.2.3.2 Interpretation

This facies association is interpreted as being deposited in proximal delta-front environments, under higher energy flow compared to the distal delta-front deposits, in agreement with comparable studies of similar facies associations (Fielding, 2010; Hampson et al., 2011; Forzoni et al., 2015). The mudstones have been entirely eroded by the frequent sandy beds. The thicker sandy beds contain larger-scale sedimentary structures, formed by migration of larger-scale dunes and sediment gravity flows. Previous authors deduced that similar sediments were transported towards the basin by subaqueous terminal distributary channels (Bhattacharya, 2006; Olariu and Bhattacharya, 2006). The wide range of palaeocurrent directions may relate to the multiplication of the active terminal distributary channels due to deltaic progradation, as seen in other deltas (Olariu and Bhattacharya, 2006).

5.2.4 Delta-top facies association

The fourth facies association regroups four different facies, deposited under specific sedimentary processes, in the same depositional environment.

5.2.4.1 Interdistributary bay facies

5.2.4.1.1 Description

The sediments deposited in the first facies consist of 1 to 5m-thick sandstones, directly overlying pro-delta facies. The greenish-gray (GLEY1-5/5GY), moderately sorted, sandstones have low sphericality and are sub-angular. The sandstones Sm form meter-thick continuous layers with a diffuse base (Fig. 10e). The layers coarsen upwards from very-fine to medium grain-sizes towards the top of the sandy beds. The sandstones are massive and structureless. A few, decimeter-scale troughs randomly occur in these beds. The troughs are filled in with millimeter-scale terrestrial organic material fragments. The sandstones include some well-preserved *in situ* fresh-water molluscs, such as unionids or viviparids (Tab. 4 & Fig. 5 respectively 7 and 33, 34). They also contain many vertical and horizontal burrows 0.5 to 1cm wide and 5 to 10cm deep, made by *Cruziana* ichnofossils, such as *Cylindrichnus*.

5.2.4.1.2 Interpretation

This facies has been formed by the deposition of fine-grained sediments out of suspension, under low energy conditions and in low salinity. These environmental conditions are corroborated by the presence of fresh-water molluscs, burrows, and terrestrial organic material.

In line with previous studies (Elliott, 1974; Overeem et al., 2003), this facies was interpreted to be deposited in interdistributary bay environments, in-between distributary channels. Sand laden currents entered and progressive encroached the interdistributary bay, producing a coarsening upwards succession. Finer-scale sedimentary structures and thin intervening bay mudstones and sandstones were probably erased by intensive bioturbation.

5.2.4.2 Distributary mouth bar facies

5.2.4.2.1 Description

The second facies forms 2 to 5m-thick sandstone beds. The grayish-brown (2.5Y-5/2), fine to medium-grained sandstones are moderately-sorted and comprise low-sphericality and sub-angular quartz grains. They form meter-scale beds with weak inverse grading from the base to the center of the beds and weak normal grading from the middle to the top of the beds. The sandstones contain 4 types of decimeter- to meter-scale cross-bedding. Facies Sr displays 10 to 50cm-thick climbing ripples at the bases and/or at the tops of the sandy beds (Fig. 11b). Facies Ss contains 50 to 100cm-thick sigmoidal cross-stratification (Fig. 11c). Facies Sl encloses 50 to 200cm-thick low-angle cross-stratification (Fig. 10f). Finally, facies Sh displays millimeter-scale horizontal laminations (Fig. 10g). The foresets of the cross-beddings are draped by laminae of millimeter-scale terrestrial organic material fragments (Fig. 13a, 13b). Some centimeter-scale clay pebbles are sometimes found at the base of this facies. This facies displays palaeocurrent directions with a mean

direction of 165° (n=5; Fig. 12c) and a range from 0° to 210°.

FIGURE 13

5.2.4.2.2 Interpretation

This facies is interpreted to be formed in distributary mouth bars, under high energy depositional processes. The clay pebbles present at the base of the sand beds were likely formed by erosion of the underlying muddy substratum due to scouring of relatively high-energy streams. The energy flow progressively increased from the base up to the middle of the sandy beds, generating the inverse grading. It then gradually decreased from the middle up to the top of the sandy beds, generating normal grading. The climbing ripples at the bases and tops of these beds were likely formed by migration of small-scale current ripples, whereas the larger-scale cross-bedding in the middle parts of these beds formed by migration of large-scale dunes.

In comparison to similar studies on comparable facies (Forzoni et al., 2015), we interpreted these deposits as being formed by the lateral and longitudinal accretion of distributary mouth bars. This bi-directional accretion supposedly created the wide range of palaeocurrent directions. Unfortunately, the available amount of data is insufficient to prove or disprove this bi-directionality.

5.2.4.3 Channel fill facies

5.2.4.3.1 Description

The third facies displays 2 to 3m-thick sandstones forming several decimeter-thick layers. The grayish-brown (2.5Y-5/2), fine-grained sandstones are moderately sorted, have low-

sphericality and are sub-angular. The sandstones show a haphazard succession of various centimeter-scale cross-bedding types (Sc, Sh, Sr, Sl). They contain asymmetrical current ripples with an amplitude of 3 to 5cm and a wavelength of 7 to 10cm (Fig. 11a), horizontal millimeter-scale laminations (Fig. 10g), 10 to 50cm-thick climbing ripples (Fig. 11b), and occasionally 30 to 50cm-thick low-angle cross-stratification (Fig. 10f). The foresets of the cross-beds and the horizontal laminations are draped by laminae of millimeter-scale terrestrial organic material fragments.

5.2.4.3.2 Interpretation

These sandstones are gradually deposited on top of the distributary mouth-bar deposits. They display various sedimentary structures that are formed by migration of small-scale current ripples or by deposition of fine sediment out of suspension. The enrichment in terrestrial organic material draping the sedimentary structures is indicative of waxing and waning of the fluvial flow. Sediment were deposited under fluctuating current velocities.

According to work on similar facies (Elliott, 1974; Fielding, 1986; Bhattacharya, 2006), this facies was interpreted as the infill of a channel, progressively submitted to avulsion.

5.2.4.4 Coastal-plain mire facies

5.2.4.4.1 Description

The last facies includes 0.2 to 0.5m-thick structureless clays (C). These clays are very-dark-gray (GLEY1-3/N) and are rich in dispersed millimeter- to decimeter-scale terrestrial organic

material fragments (Fig. 10a). The clays contain some well-preserved, *in situ*, fresh-water molluscs, such as unionids (*Rumanunio rumanus*), viviparids or pachychilids (*Tinnyea abchasica*) (Tab. 4 & Fig. 5). The top of the clays are occasionally showing centimeter-scale ichnofossils, such as *Planolites*, forming horizontal burrows of 0.5 to 1cm wide and 1 to 3cm deep. More rarely, the top of these clays display vertical roots of 0.5 to 1cm wide and 5 to 10cm deep. The upper 5 to 10 centimeters of this facies are occasionally indurated.

5.2.4.4.2 Interpretation

The organic-rich mudstones are interpreted as having been deposited out of suspension, in low-energy coastal-plain mires. The upper parts of this facies, affected by burrows and roots, point to sporadic, subaerial exposure of the environments. More prolonged subaerial exposure may have indurated the upper parts of these deposits.

In line with previous studies of similar facies (Fielding, 2010; Hampson, 2010; Forzoni et al., 2015), we interpreted these organic-rich layers to be deposited on coastal-plain mires during fluvial flooding.

5.2.5 Flooding surfaces

5.2.5.1 Description

The fifth facies association consists of 0.2 to 0.4m-thick sandstones. The sandstones Sfr form decimeter-thick layers with wavy, sharp, erosive bases (Fig. 11f). The sediments are quartz-rich with highly spherical and sub-angular grains. They are medium- to coarse-grained and well-sorted sandstones. The

777 weathered surfaces of these sandstones have a noticeable
778 reddish-brown color (2.5YR-4/4), whereas the fresh surface is
779 more grayish (GLEY1-4/N). The sandstones are mostly
780 structureless, but occasionally show centimeter- to decimeter-
781 scale low-angle cross-stratification. Microscopic observations
782 realized on thin-sections show enrichment in sub-angular
783 glauconite grains in these sands (Fig. 13c, 13d). The macroscopic
784 and microscopic observations of these sandstones display high
785 concentrations of shells fragments dispersed in the sediment.
786 The shells are abraded or broken, and composed of a mix
787 between brackish- and fresh-water molluscs (Tab. 4 & Fig. 5).
788 The sandstones display iron cement, that is post-diagenetically
789 oxidized, distributed throughout the entire sand bed, leading to
790 the formation of indurated layers.

791 ***5.2.5.2 Interpretation***

792 These sandstones correspond to flooding surfaces, created
793 under high-energy depositional processes. The formation of
794 erosive sand beds, including mature sands and many abraded
795 and reworked shells, required erosion and sediment reworking
796 along the shoreface (Weimer, 1988; Scarponi et al., 2013). The
797 formation of glauconite necessitates slow sedimentation rates
798 down to slight erosion (Cloud, 1955). Winnowing processes may
799 have diminished the sedimentation rate and caused episodic
800 sediment starvation (Kidwell and Aigner, 1985; Brett, 1995),
801 leading to the formation of condensed layers (Kidwell, 1989;
802 Abbott and Carter, 1994; Brett, 1995; Scarponi et al., 2013).

803 Alike previous interpretations of such oxidized shell-rich
804 layers (Nummedal and Swift, 1987; Weimer, 1988; Murakoshi
805 and Masuda, 1992; Cattaneo and Steel, 2003; Hurd et al., 2014),
806 we interpreted this facies as flooding surfaces. Along our section
807 these deposits display a red weathering color and are cemented,
808 which is probably the result of post-diagenetic oxidation during
809 sub-aerially exposure. FIGURE 14

810 5.3 Delta stratigraphy

811 5.3.1 Parasequences

812 Throughout the entire section, the facies associations tend
813 to always appear in the same stratigraphic order, forming 5 to
814 40m-thick sedimentary successions (Fig. 14). These sedimentary
815 successions begin with 1 to 13m-thick pro-delta massive or
816 laminated mudstones (Fig. 14 - Logs A-F). The pro-delta deposits
817 are overlain by 1 to 5m-thick distal delta-front mudstones with
818 thin sandy intercalations (Fig. 14 - Logs A, C-F). The transition
819 from distal delta-front to proximal delta-front is marked by a
820 progressive coarsening-up and the deposition of 0.5 to 3m-thick
821 small-scale cross-bedded sandstones with thin muddy
822 intercalations (Fig. 14 – C-F). Successions continue upwards with
823 several delta-top deposits. Delta-top sediments occasionally
824 correspond to 1 to 5m-thick massive sandstones deposited in
825 interdistributary bays (Fig. 14 - Log B). These sandstones are
826 deposited directly on top of the pro-delta and delta-front
827 sediments. They mark the transition from distal to shallower and
828 more restricted depositional environments, without recording
829 any dynamic, deltaic, sandy input. On other occasions, the deltaic

input is recorded and pro-delta and delta-front sediments are overlain by 2 to 7m-thick distributary mouth bars, forming large-scale cross-bedded sandstones (Fig. 14 - Log C, E-F). These distributary mouth bars sometimes erode the underlying proximal delta-front and are directly deposited on top of distal delta-front deposits (Fig. 14 - Log A). The distributary mouth bars are infrequently overlain by 1 to 3m-thick channel fill deposits, creating small-scale cross-bedded organic-rich sandstones (Fig. 14 - Log C) or 0.2 to 0.5m coastal-plain mire deposits, forming bioturbated organic-rich clays (Fig. 14 - Log E).

Each sedimentary succession displays a shallowing-upward trend, regressing from deeper open-water towards shallow fluvial environments. These regressive successions are bounded by oxidized, shell- and glauconite-rich flooding surfaces (Fig. 14 - Log A-C, E-F). These flooding surfaces were formed during relative water-level transgressions, corresponding to delta-lobe switching, which formed in total 64 shallowing-upwards successions, defined in the literature as parasequences (Catuneanu et al., 2011). These 64 parasequences are illustrated in the relative water-level curve, based on attributing a depth rank to the facies associations (Fig. 3b). This curve highlights numerous relative water-level variations of low magnitude.

5.3.2 Sequences

The relative water-level curve displays likewise relative water-level variations of higher magnitude. The 64 parasequences can be stacked in larger-scale regressive events (Fig. 3b). In other well documented cases, these larger-scale

857 events are bounded by major unconformities usually correlated
858 throughout the entire basin and defined in the literature as
859 sequences (Catuneanu et al., 2011).
860 In our section, the parasequences can be grouped into 9 low-
861 order regressive sequences, each of them enclosing between 17
862 to 29 regressive parasequences. The low-order regressive
863 sequences are delimited by well-developed delta-top facies, such
864 as meter- to decameter-thick distributary mouth bars or channel
865 fill deposits. The low-order sequences can themselves be stacked
866 into 3 high-order regressive sequences. Each high-order
867 regressive sequence encloses 3 regressive low-order sequences.
868 The high-order regressive sequences are bounded by even
869 shallower delta-top facies, such as decameter-thick channel fills
870 or decimetre- to meter-thick coastal-plain mire deposits, marked
871 by important enrichment in terrestrial organic material,
872 ichnofossils and fresh-water faunas. These low- and high-order
873 sequences highlight larger scale regressive events, related to
874 larger relative water-level variations in the basin.

875 ### 5.3.3 Large-scale trends

876 The general regression of the entire deltaic system is
877 interrupted by rhythmic relative water-level variations of
878 various amplitudes, as illustrated in the relative water-level
879 curve illustrates (Fig. 3b).
880 The base of the section is mostly mud dominated. The 15m-
881 thick parasequences are on average composed of 77%
882 mudstones (Fig. 15). These muddy regressive parasequences
883 start with meter- to decameter-thick pro-delta deposits, showing

numerous gravity currents and hyperpycnal flows (Fig. 15a). Pro-delta deposits are overlain by meter-thick distal delta-front deposits, often disturbed by convolute bedding (Fig. 15b). The succession regresses up to decimeter-thick proximal delta-front deposits, forming thin sandy beds with small-scale sedimentary structures (Fig. 15c). Delta-top deposits hardly occur in the basal part of the section. Furthermore, parasequences are at the base grouped in 94 to 137m-thick low-order sequences and in 350m-thick high-order sequences (Fig. 3b). FIGURE 15/FIGURE 16

Towards the top of the section, the parasequences are on average composed of 56% mudstones, whereas the amount of sand has doubled compared to the base of the section (Fig. 16). In these sandy, regressive parasequences, the pro-delta deposits are only decimeter- to meter-thick, or are absent. They are overlain by decimeter- to meter-thick distal delta-front deposits, showing frequent gravity currents (Fig. 16a). On top of them, meter-thick proximal delta-front deposits are found, with meter-thick sandstone layers containing large-scale sedimentary structures. These sandy parasequences commonly regress up to meter-thick erosional distributary mouth bar deposits (Fig. 16b), or more rarely into meter-thick channel fill deposits. They are occasionally capped by centimeter- to decimeter-thick coastal-plain mire deposits, showing organic-rich sediments with roots and burrows (Fig. 16c). The thickness of the parasequences decreases down to 9m towards the top of the section. These thinner parasequences are also grouped into thinner low- and high-order sequences. The low-order sequences thickness

decreases down to 65 to 121m and the high-order sequences thickness decreases down to 208m (Fig. 3b). TABLE 5

5.4 Controls on deltaic progradation

The deltaic progradation formed numerous regressive parasequences and sequences, generated by frequent delta-lobe switching. Thanks to the robust time frame available for this section, it is possible to test if the rhythmicity of this delta is autogenic or allogenic (Fig. 2c & Fig. 2d).

Firstly, the 64 parasequences highlight small-scale relative water-level variations with a frequency of 12 ± 9kyr. They occur too frequently to be coeval to any climatic cycles. The 13.6-25m and 25-37m filters are indeed not in range with the 23kyr precession cycles (Fig. 17). On a larger scale, the 64-111m and 50-138m filters could potentially be correlated with the 40kyr obliquity cycles. However, the correlation between their frequencies is not very convincing. Secondly, the 9 low-order sequences display a frequency of 81 ± 44kyr. Even if they are in range with the 100kyr eccentricity cycles, these events occur too frequently and do not match to these cycles (Fig. 17). Finally, the 3 high-order sequences have a frequency of 243 ± 61kyr. These major sequences occur too frequently to be linked to the 400kyr eccentricity cycles (Fig. 17). In summary, it seems that neither the parasequences nor the sequences are coeval to astronomical climatic forcing.

The sedimentary succession, however, records several hiatuses, which might affect the time frame of the deltaic progradation. Firstly, each parasequences is topped by a minor

hiatus. The parasequence boundaries are indeed marked by shell-rich oxidized layers, formed under sediment starvation during the flooding events. Moreover, a level that is interpreted as a larger hiatus was observed at around 250m in the section, delimiting two low-order sequences. The boundary between these two low-order sequences is marked by a series of four shell-rich oxidized layers. We estimate that around 40m of sediments were eroded. This major hiatus correlates with a dramatic drop of the sedimentation rate, going from 125cm/kyr down to 65cm/kyr in this part of the section (Fig. 18). Even if the section displays some hiatuses, the parasequences and sequences are most likely the result of autogenic relative water-level variations. FIGURE 17

6 Discussion

6.1 The Slănicul de Buzău section: a typical example of a river-dominated delta

The Slănicul de Buzău section highlights a coarsening-upward of the sediments and a thinning of the regressive parasequences and sequences towards the top. This trend demonstrates an increase in the energy of the depositional processes and a decrease in the accommodation space, with a system less and less in balance. This general regression occurred due to deltaic progradation progressively filling the sedimentary basin. According to the classification of Galloway (1975), the studied deltaic system shaped a river-dominated delta. The

963 sediments display a strong river influence, related to an
964 important sedimentation rate of 152cm/kyr on average. In the
965 older part of the section, sediments have been preferentially
966 transported into the basin through gravity currents and
967 hyperpycnal flows, whereas towards the younger part, they have
968 progressively been transported by transcontinental flows. The
969 sediment supply has fed a multitude of deltaic lobes and
970 distributary channels, covering a wide distributary area. The
971 deltaic system doesn't display any evidence for tide interference
972 and minor wave activity. There is no evidence of sediment
973 redistribution expect during the flooding events, no sand spit
974 formation, symmetrical wave structures or clay draping on the
975 sediment foresets. In the absence of these features, this
976 sedimentary system is interpreted as a strictly river-dominated
977 delta.

978 ## 6.2 Distinctive deltaic characteristics in semi-
979 isolated basins

980 The delta system preserved in the Slănicul de Buzău section
981 prograded into a semi-isolated basin and this unusual
982 depositional environment strongly influenced the deltaic
983 architecture and the sedimentary facies.

984 Firstly, the restricted Dacian Basin formed a protected
985 depositional environment. In this semi-isolated basin, wave and
986 tide activity were limited due to the restricted connectivity with
987 the open ocean. In fact, there is very little evidence of sediment
988 instability. This is probably due to the low energy in this semi-
989 isolated environment, preventing any sediment reworking.

990 However, the absence of indications of wave and tide influence
991 could also be partly due to the very strong river input into the
992 basin.
993 Secondly, the isolation nature of the basin engendered
994 lowered salinities (Popov et al., 2006; Leever et al., 2009; Stoica
995 et al., 2013), and by association, lowered water densities. Low
996 density water bodies are more susceptible to support sediment
997 transport by hyperpycnal plumes (Sturm and Matter, 1978;
998 Mulder et al., 2003). These fine-grained organic-rich deposits are
999 very frequent in our section. Organic material was also found on
1000 the foresets of the cross-bedded sandstones, underlining a
1001 proximal low energy depositional setting. Furthermore, the
1002 section records numerous ichnofossils, in particular in the
1003 interdistributary bays and coastal-plain mires. The development
1004 of ichnofossils is known to be favored by low salinity (Bohacs et
1005 al., 2003). Moreover, these low salinities encouraged the mixture
1006 of brackish- and fresh-water faunas observed. Our section is
1007 extremely rich in faunas, which are also sometimes found *in situ*.
1008 The preservation of all these features has been ensured by the
1009 relatively low depositional energy, as well as limited erosional
1010 processes in the studied semi-isolated basin.
1011 Thirdly, it appears that the delta prograded into a shallow
1012 environment, on a low-angle slope. Shallow basins are often
1013 influenced by reinforced wave action (De Raaf et al., 1977;
1014 Hampson et al., 2011; Forzoni et al., 2015). Here, the fluvial
1015 influence was clearly dominant and suppressed most of the wave
1016 influence. The deposits were nevertheless occasionally disturbed

1017 by minor wave and storm action, creating small-scale lenticular
1018 bedding and thin, shell-rich storm deposits. To be affected by
1019 these processes, we estimate that the depositional depth must
1020 have been at least 20m. The deltaic progradation in this shallow
1021 basin with a low-gradient slope forms thin sand bodies with an
1022 average thickness of 1 to 2m, whereas they can be decameter-
1023 thick in the open ocean (e.g. Olariu and Olariu, 2015). Sediments
1024 deposited in these environments are also known to form sharply-
1025 based sand bodies, with small-scale cross-bedding (Fielding,
1026 2010; Vincent et al., 2010). In line with this study, the sand
1027 bodies in our section are often erosive at their bases and only
1028 comprise decimeter- to meter-thick cross-bedded strata. Due to
1029 the lack in accommodation space, the deltaic progradation
1030 subsequently generated numerous thin regressive
1031 parasequences. The parasequences are on average only 13.5m-
1032 thick in our section. In shallow environments the parasequences
1033 are known to be generally relatively thin (Bohacs et al., 2000;
1034 Sztanó et al., 2013), whereas they can form up to hundreds
1035 meter-thick sediment succession in the open ocean (e.g. Olariu
1036 and Olariu, 2015). The more distal parasequences at the base of
1037 our section are on average about 5m thicker than the proximal
1038 ones at the top of the section, showing the gradual decrease of
1039 accommodation space through time. Parasequences were formed
1040 by frequent migration of numerous small distributary channels.
1041 These distributary channels were affected by repetitive delta-
1042 lobe switching, covering a wide range of palaeocurrent
1043 directions. The formation of a wider distributary area can be

enhanced by low gradient slopes (Bhattacharya, 2006; Olariu and Bhattacharya, 2006).

The delta-lobe switching was strictly controlled by autogenic processes. Neither the frequencies of the parasequences, low-order sequences nor high-order sequences were in line with astronomical climatic forcing (Fig. 17). Conversely, further to the north, in the Putna and Râmnicu Sărat sections, the proximal deltaic evolution seems to have been affected by astronomical precession cycles (Vasiliev et al., 2004). This suggests Milankovitch climate cycles can be registered in river-dominated deltas (Sacchi and Müller, 2004; e.g. Li and Bhattacharya, 2013), but that towards more distal areas, climate forcing of river-dominated deltas become progressively overridden by autogenic processes due to more frequent delta-lobe switching, as suggest by previous researches (Castelltort and Van Den Driessche, 2003). FIGURE 18

On the low-gradient margin of this shallow basin, recurrent autogenic delta-lobe switching repetitively creates relative water-level rise and produces frequent flooding surfaces. When the progradation of a deltaic lobe fills the local accommodation space, this lobe is abandoned to the benefit of another lobe, which then progrades laterally to the first one, towards a location with still some accommodation space left. The upper surface of the abandoned lobe then records a flooding event, which enhances sediment starvation and winnowing. In restricted basins, these processes often lead to the formation of condensed shell-rich layer, enriched in glauconite (Cloud, 1955; Cattaneo

and Steel, 2003). Once sub-aerially exposed, the glauconite is then oxidized, forming reddish indurated layers.

To summarize, the delta system preserved in the Slănicul de Buzău section was prograding into a semi-isolated basin, forming a protected, brackish, shallow depositional environment with a low-gradient slope. In our opinion, this delta is comparable to the recent Kura Delta in the Caspian Sea, or, in a non-uplifting context, to the Mediterranean Nile Delta or, in a more open marine context, to the Mackenzie Delta in the Beaufort Sea. According to the delta classification of Galloway (1975), this delta is a river-dominated delta. However, in restricted basins where wave and tide interferences are weak or even absent, this classification does not seem the most appropriate. A more relevant classification might be the one from Postma (1995), who considers the sedimentary architecture of river-dominated deltas depending of the water depths and the gradients of the basin. In regards to this classification, the studied delta would be interpreted as a mouth bar-type delta with a Gilbert-type profile. Further researches are nevertheless necessary to improve our understanding in term of sedimentary architecture and depositional processes of deltaic system evolving in (semi-)isolated basins.

6.3 Evolution of the mid-Pliocene Dacian Basin

During the mid-Pliocene Dacian stage, the Dacian Basin received the erosion products of the uplifting Carpathians (Fig. 1). The Eastern part of the Carpathians was drained by a river flowing parallel to the mountain belt (Jipa, 1997; Popov et al.,

2006; Jipa and Olariu, 2009; Leever et al., 2009; Stoica et al., 2013; Fongngern et al., 2016; Matoshko et al., 2016). This river prograded southwards, with a mean palaeocurrent direction of 195° (Fig. 12d). This southwards flowing river generated a north to south thinning of the sand bodies and a decrease in grain sizes. In the northern Putna section (Jipa and Olariu, 2009), the sand bodies are around 5m-thick and composed of coarse-grained sediments (Vasiliev et al., 2004). The Râmnicu Sărat section, 35km to the south, displays 2 to 3m-thick sand bodies (Jipa and Olariu, 2009), composed of medium-grained sediments (Vasiliev et al., 2004). In the southernmost Slănicul de Buzău section, located 50km south of the Putna section, the sand bodies are only 1 to 2m-thick and are composed of fine-grained sediments. The depositional environment was therefore becoming progressively more distal southwards, with the development of a river dominated delta prograding on the northern margin of the Dacian Basin.

This deltaic system remained relatively stable during the entire Dacian stage leading to the deposition of 835m of deltaic sediments in around 0.6 Ma (Fig. 3a). This major storage of sediments was ensured by the equilibrium between subsidence and sedimentation rates (Bertotti et al., 2003). The regional subsidence rate of 90cm/kyr (Tărăpoancă et al., 2003) was balanced by average sedimentation rates of 90cm/kyr in the more northern Râmnicu Sărat section (Vasiliev et al., 2004) and of 139cm/kyr in the Slănicul de Buzău section (Fig. 13). The delta prograded on the northern margin of the Dacian Basin towards

1125 the deep Southern foreland depression. The deltaic progradation
1126 shaped a general shallowing-upward succession, marked by an
1127 increase of coarser material. The succession similarly registered
1128 a general freshening-upward trend with an increasing
1129 contribution of fresh water elements, which is in agreement with
1130 previous bio-stratigraphic studies (Andreescu et al., 2011; Van
1131 Baak et al., 2015). The basin became filled during the Romanian
1132 (Jipa and Olariu, 2009), when sedimentation progressively
1133 stopped in this area. Consequently, the Dacian deltaic system
1134 merged with the Danube Delta prograding eastwards along the
1135 southern Carpathians. The Dacian Basin must have become
1136 overfilled soon after, because both provenance analyses and a
1137 change in depositional style in the NW Black Sea deep-water fan
1138 indicate that the Danube River started to supply sediment to the
1139 Black Sea around 4 Ma ago (De Leeuw et al., 2017 *accepted*;
1140 Olariu et al., 2017 *accepted*).
1141 During the Dacian, a thick deltaic progradation sequence
1142 was recorded, represented by parasequences topped by oxidized
1143 indurated shell layers. Similar iron-rich layers are not observed
1144 during the preceding Pontian regional stage, suggesting the
1145 presence of highly specific environmental conditions during the
1146 Dacian, in which the water depth was favorable to the formation
1147 of these layers on top of the delta-lobes. The high quantities of
1148 glauconite and abundant organic material found in this part of
1149 the section suggest increased runoff in response to the higher
1150 temperatures during the Pliocene (Fedorov et al., 2013). In fact,
1151 similar iron-rich sediments are present in other locations around

the Black Sea during the Pliocene (Nevesskaya et al., 2003; Krijgsman et al., 2010). Increased temperatures during the Pliocene could also have caused increased weathering of adjacent land-areas, leading to an increased iron content of the waters in the concerned basins (Muratov, 1964). The depositional controls of these layers are still not well understood and additional research is needed to better understand their specifics.

7 Conclusion

During the Pliocene, the Dacian Basin was an embayment of the Black Sea. The northern shelf of this semi-isolated basin was supplied by a delta flowing southward along the Eastern Carpathians. This delta prograded on a low-gradient slope into this shallow brackish-water basin, where it constructed a strongly river-dominated delta system. This unique depositional environment highlights a particular internal sedimentary architecture, which differs from a typical open ocean delta. The deltaic progradation shaped a multiplication of small terminal distributary channels. They experienced frequent delta-lobe switching, creating numerous thin regressive parasequences overlain by oxidized shell-rich and glauconite-rich flooding surfaces. This study displays a deltaic evolution mainly forced by internal processes, generating an autogenic river-dominated delta. The delta remained exclusively influenced by fluvial processes until the total infill of the Dacian Basin at the base of the Romanian stage.

Acknowledgments

This research was supported by the project PRIDE (Pontocaspian RIse and DEmise), which has received funding from the European Union's Horizon 2020 research and innovation program, under the Marie Sklodowska-Curie [grant agreement No 642973]. Our partner institute CASP, where part of the research has been conducted, is specially thanked for its hospitality and cooperation.

References

Abbott, S.T., Carter, R.M., 1994. The Sequence Architecture of Mid-Pleistocene (c. 1.1–0.4Ma) Cyclothems from New Zealand: Facies Development during a Period of Orbital Control on Sea-Level Cyclicity. Special Publication International Association of Sedimentologists 19, 367–394.

Abels, H.A., Aziz, H.A., Ventra, D., Hilgen, F.J., 2009. Orbital Climate Forcing in Mudflat to Marginal Lacustrine Deposits in the Miocene Teruel Basin (Northeast Spain). Journal of Sedimentary Research 79, 831–847. https://doi.org/10.2110/jsr.2009.081

Abels, H.A., Aziz, H.A., Krijgsman, W., Smeets, S.J.B., Hilgen, F.J., 2010. Long-period eccentricity control on sedimentary sequences in the continental Madrid Basin (middle Miocene, Spain). Earth and Planetary Science Letters 289, 220–231. https://doi.org/10.1016/j.epsl.2009.11.011

Allen, M.B., Armstrong, H.A., 2008. Arabia – Eurasia collision and the forcing of mid-Cenozoic global cooling. Palaeogeography, Palaeoclimatology, Palaeoecology 265, 52–58. https://doi.org/10.1016/j.palaeo.2008.04.021

Allmendinger, R.W., Cardozo, N., Fisher, D.M., 2011. Structural Geology Algorithms. Vectors and Tensors. Cambridge University Press, Cambridge, 302.

Andreescu, I., Codrea, V., Enache, C., Lubenescu, V., Munteanu, T., Petculescu, A., Stiuca, E., Terzea, E., 2011. Reassessment of the Pliocene/Pleistocene (Neogene/Quaternary) boundary in the Dacian Basin (Eastern Paratethys), Romania. Muzeul Olteniei Craiova 27, 197–220.

Andrews, S.D., Moreau, J., Archer, S., Bristow, C., 2016. Devonian lacustrine shore zone architecture: Giving perspective to cliff

1214 exposures with ground penetrating radar. Sedimentology 63,
1215 2087–2105. https://doi.org/10.1111/sed.12297
1216 Barth, G., Franz, M., Heunisch, C., Kustatscher, E., Thies, D., Vespermann,
1217 J., Wolfgramm, M., 2014. Late Triassic (Norian-Rhaetian) brackish
1218 to freshwater habitats at a fluvial-dominated delta plain
1219 (Seinstedt, Lower Saxony, Germany). Palaeobiodiversity and
1220 Palaeoenvironments 94, 495–528.
1221 https://doi.org/10.1007/s12549-014-0168-6
1222 Bertotti, G., Maţenco, L., Cloetingh, S., 2003. Vertical movements in and
1223 around the south-east Carpathian foredeep: Lithospheric memory
1224 and stress field control. Terra Nova 15, 299–305.
1225 Bhattacharya, J.P., 2006. Deltas. SEPM Special Publication 84, 237–292.
1226 https://doi.org/10.2110/pec.06.84.0237
1227 Bhattacharya, J.P., MacEachern, J., 2009. Hyperpycnal Rivers and
1228 Prodeltaic Shelves in the Cretaceous Seaway of North America.
1229 Journal of Sedimentary Research 79, 184–209.
1230 https://doi.org/10.1111/joa.12085
1231 Bohacs, K.M., Carroll, A.R., Neal, J.E., 2003. Lessons from large lake
1232 systems-Thresholds, nonlinearity, and strange attractors.
1233 Geological Society of America Special Papers 270, 75–90.
1234 https://doi.org/10.1130/0-8137-2370-1.75
1235 Bohacs, K.M., Carroll, A.R., Neal, J.E., Mankiewicz, P.J., 2000. Lake-Basin
1236 Type, Source Potential, and Hydrocarbon Character: An Integrated
1237 Sequence-Stratigraphic-Geochemical Framework, in: Gierlowski-
1238 Kordesch, E.H., Kelts, K.R. (Eds.), Lake Basins Through Space and
1239 Time. AAPG Studies in Geology, 3–34.
1240 https://doi.org/http://dx.doi.org/10.1306/E4FD42AB-1732-
1241 11D7-8645000102C1865D
1242 Brett, C.E., 1995. Sequence stratigraphy, biostratigraphy,and
1243 taphonomy in shallow marine environments. Palaios 10, 597–616.

1244 Cardozo, N., Allmendinger, R.W., 2013. Spherical projections with
1245 OSXStereonet. Computers and Geosciences 51, 193–205.
1246 https://doi.org/10.1016/j.cageo.2012.07.021
1247 Castelltort, S., Van Den Driessche, J., 2003. How plausible are high-
1248 frequency sediment supply-driven cycles in the stratigraphic
1249 record? Sedimentary Geology 157, 3–13.
1250 https://doi.org/10.1016/S0037-0738(03)00066-6
1251 Cattaneo, A., Steel, R.J., 2003. Transgressive deposits: A review of their
1252 variability. Earth-Science Reviews 62, 187–228.
1253 https://doi.org/10.1016/S0012-8252(02)00134-4
1254 Catuneanu, O., Galloway, W.E., Kendall, C.G.S.C., Miall, A.D., Posamentier,
1255 H.W., Strasser, A., Tucker, M.E., 2011. Sequence Stratigraphy:
1256 Methodology and Nomenclature. Newsletters on Stratigraphy 44,
1257 173–245. https://doi.org/10.1127/0078-0421/2011/0011
1258 Cloetingh, S.A.P.L., Burov, E., Matenco, L., Toussaint, G., Bertotti, G.,
1259 Andriessen, P.A.M., Wortel, M.J.R., Spakman, W., 2004. Thermo-
1260 mechanical controls on the mode of continental collision in the SE
1261 Carpathians (Romania). Earth and Planetary Science Letters 218,
1262 57–76. https://doi.org/10.1016/S0012-821X(03)00645-9
1263 Cloud, P.E.J., 1955. Physical limits of glauconite formation. American
1264 Society of Petroleum Geologists. Bulletin 39, 484–492.
1265 Cohen, A.S., 2012. Scientific drilling and biological evolution in ancient
1266 lakes: Lessons learned and recommendations for the future.
1267 Hydrobiologia 682, 3–25. https://doi.org/10.1007/s10750-010-
1268 0546-7
1269 Cohen, K.M., Finney, S.C., Gibbard, P.L., Fan, J.-X., 2013. The ICS
1270 International Chronostratigraphic Chart (updated). Episodes 36,
1271 199-204.
1272 Constantinescu, A.M., Toucanne, S., Dennielou, B., Jorry, S.J., Mulder, T.,
1273 Lericolais, G., 2015. Evolution of the danube deep-sea fan since the

1274 last glacial maximum: New insights into Black Sea water-level
1275 fluctuations. Marine Geology 367, 50–68.
1276 https://doi.org/10.1016/j.margeo.2015.05.007
1277 De Leeuw, A., Morton, A., Van Baak, C.G.C., Vincent, S.J., 2017. Timing of
1278 arrival of the Danube to the Black Sea : Provenance of sediments
1279 from DSDP Site 380/380A. Terra Nova.
1280 De Raaf, J.F.M., Boersma, J.R., Van Gelder, A., 1977. Wave-generated
1281 structures and sequences from a shallow marine succession,
1282 Lower Carboniferous, County Cork, Ireland. Sedimentology 24,
1283 451–483. https://doi.org/10.1111/j.1365-3091.1977.tb00134.x
1284 Dumitrescu, I., Săndulescu, M., Bandrabur, T., 1970. Geological map,
1285 Scale 1:200.000, sheet 29 Covasna. Geological Institute of
1286 Romania, Bucharest.
1287 Dupont-Nivet, G., Vasiliev, I., Langereis, C.G., Krijgsman, W., Panaiotu, C.,
1288 2005. Neogene tectonic evolution of the southern and eastern
1289 Carpathians constrained by paleomagnetism. Earth and Planetary
1290 Science Letters 236, 374–387.
1291 https://doi.org/10.1016/j.epsl.2005.04.030
1292 Elliott, T., 1974. Interdistributary bay sequences and their genesis.
1293 Sedimentary Geology 21, 611–622.
1294 Fedorov, A. V., Brierley, C.M., Lawrence, K.T., Liu, Z., Dekens, P.S., Ravelo,
1295 A.C., 2013. Patterns and mechanisms of early Pliocene warmth.
1296 Nature 496, 43–49. https://doi.org/10.1038/nature12003
1297 Fielding, C.R., 1986. Fluvial channel and overbank deposits from the
1298 Westphalian of the Durham coalfield, NE England. Sedimentology
1299 33, 119–140. https://doi.org/10.1111/j.1365-
1300 3091.1986.tb00748.x
1301 Fielding, C.R., 2010. Planform and Facies Variability in Asymmetric
1302 Deltas: Facies Analysis and Depositional Architecture of the
1303 Turonian Ferron Sandstone in the Western Henry Mountains,

South-Central Utah, U.S.A. Journal of Sedimentary Research 80, 455–479. https://doi.org/10.2110/jsr.2010.047

Fongngern, R., Olariu, C., Steel, R.J., Krézsek, C., 2016. Clinoform growth in a Miocene, Para-tethyan deep lake basin: thin topsets, irregular foresets and thick bottomsets. Basin Research 28, 770–795. https://doi.org/10.1111/bre.12132

Fongngern, R., Olariu, C., Steel, R., Mohrig, D., Krézsek, C., Hess, T., 2017. Subsurface and outcrop characteristics of fluvial-dominated deep lacustrine clinoforms. Sedimentary Geology. https://doi.org/10.1111/sed.12430

Forzoni, A., Hampson, G., Storms, J., 2015. Along-Strike Variations in Stratigraphic Architecture of Shallow-Marine Reservoir Analogues : Upper Cretaceous Panther Tongue Delta and Coeval Shoreface , Star Point. Journal of Sedimentary Research 85, 968–989. https://doi.org/10.2110/jsr.2015.69

Galloway, W.E., 1975. Process framework for describing the morphological and stratigraphic evolution of deltaic depositional systems, in: Broussard, M.L. (Ed.), Deltas: Models for Exploration. Houston Geological Society, Houston, 87–98.

Gradstein, F.M., Ogg, J.G., Schmitz, M., Ogg, G., 2012. The Geologic Time Scale 2012. Elsevier, Oxford, 1176.

Hampson, G.J., 2010. Sediment dispersal and quantitative stratigraphic architecture across an ancient shelf. Sedimentology 57, 96–141. https://doi.org/10.1111/j.1365-3091.2009.01093.x

Hampson, G.J., Gani, M.R., Sharman, K.E., Irfan, N., Bracken, B., 2011. Along-Strike and Down-Dip Variations in Shallow-Marine Sequence Stratigraphic Architecture: Upper Cretaceous Star Point Sandstone, Wasatch Plateau, Central Utah, U.S.A. Journal of Sedimentary Research 81, 159–184. https://doi.org/10.2110/jsr.2011.15

1334 Hurd, T.J., Fielding, C.R., Hutsky, A.J., 2014. Variability In
1335 Sedimentological and Ichnological Signatures Across A River-
1336 Dominated Delta Deposit: Peay Sandstone Member (Cenomanian)
1337 of the Northern Bighorn Basin, Wyoming, U.S.A. Journal of
1338 Sedimentary Research 84, 1–18.
1339 https://doi.org/10.2110/jsr.2014.3
1340 Jipa, D.C., 1997. Late Neogene-Quaternary evolution of Dacian Basin
1341 (Romania). An analysis of sediment thickness pattern. Geo-Eco-
1342 Marina 2, 23–25.
1343 Jipa, D.C., Stoica, M., Andreescu, I., Floroiu, A., Maximov, G., 2011.
1344 Zanclean Gilbert-type fan deltas in the Turnu Severin area (Dacian
1345 Basin, Romania). A critical analysis. Geo-Eco-Marina 17, 123–133.
1346 Jipa, D.C., Olariu, C., 2009. Dacian Basin. Depositional Architechture and
1347 Sedimentary History of the Paratethys Sea. Geo-Eco-Marina
1348 Special Publication, Bucharest, 268.
1349 Jipa, D.C., 2015. The identity of a Paratethys Basin. Dacian Basin
1350 configuration - Outcome of the Carpathian Fordeep along-arc
1351 migration. Geo-Eco-Marina 21, 159–166.
1352 Jobe, Z.R., Lowe, D.R., Morris, W.R., 2012. Climbing-ripple successions in
1353 turbidite systems: Depositional environments, sedimentation
1354 rates and accumulation times. Sedimentology 59, 867–898.
1355 https://doi.org/10.1111/j.1365-3091.2011.01283.x
1356 Jones, R.W., Simmons, M.D., 1996. A review of the stratigraphy of
1357 Eastern Parathethys (Oligocene-Holocene). Bulletin of the Natural
1358 History Museum London 52, 25–47.
1359 Kidwell, S.M., Aigner, T., 1985. Sedimentary dynamics of complex shell
1360 beds: implications for ecologic and evolutionary patterns, in:
1361 Bayer, U., Seilacher, A. (Eds.), Sedimentary and Evolutionary
1362 Cycles. Springer, Berlin, 382-395.
1363 Kidwell, S.M., 1989. Stratigraphic condensation of marine transgressive

records: origin of major shell deposits in the Miocene of Maryland. The Journal of Geology 97, 1–24.

Koymans, M.R., Langereis, C.G., Pastor-Galán, D., van Hinsbergen, D.J.J., 2016. Paleomagnetism.org: An online multi-platform open source environment for paleomagnetic data analysis. Computers and Geosciences 93, 127–137. https://doi.org/10.1016/j.cageo.2016.05.007

Krijgsman, W., Stoica, M., Vasiliev, I., Popov, V. V., 2010. Rise and fall of the Paratethys Sea during the Messinian Salinity Crisis. Earth and Planetary Science Letters 290, 183–191. https://doi.org/10.1016/j.epsl.2009.12.020

Kroonenberg, S.B., Alekseevski, N.I., Aliyeva, E., Allen, M.B., Aybulatov, D.N., Baba-Zadeh, A., Badyukova, E.N., Davies, C.E., Hinds, D.J., Hoogendoorn, R.M., Huseynov, D., Ibrahimov, B., Mamedov, P., Overeem, I., Rusakov, G.V., Suleymanova, S., Svitoch, A.A., Vincent, S.J., 2005. Two Deltas, Two Basins, One River, One Sea: The Modern Volga Delta as an Analogue of the Neogene Productive Series, South Caspian Basin. SEPM Special Publication 83, 231–256. https://doi.org/10.2110/pec.05.83.0231

Lamb, M.P., Mohrig, D., 2009. Do hyperpycnal-flow deposits record river-flood dynamics? Geology 37, 1067–1070. https://doi.org/10.1130/G30286A.1

Laskar, J., Fienga, A., Gastineau, M., Manche, H., 2011. La2010: a new orbital solution for the long-term motion of the Earth. Astronomy and Astrophysics 532, 1-15. https://doi.org/10.1051/0004-6361/201116836

Leever, K.A., Matenco, L., Bertotti, G., Cloetingh, S., Drijkoningen, G.G., 2006. Late orogenic vertical movements in the Carpathian Bend Zone - Seismic constraints on the transition zone from orogen to foredeep. Basin Research 18, 521–545.

https://doi.org/10.1111/j.1365-2117.2006.00306.x

Leever, K.A., Matenco, L., Rabagia, T., Cloetingh, S., Krijgsman, W., Stoica, M., 2009. Messinian sea level fall in the Dacic Basin (Eastern Paratethys): Palaeogeographical implications from seismic sequence stratigraphy. Terra Nova 22, 12–17. https://doi.org/10.1111/j.1365-3121.2009.00910.x

Leever, K.A., Matenco, L., Rabagia, T., Cloetingh, S., Krijgsman, W., Stoica, M., 2010. Messinian sea level fall in the Dacic Basin (Eastern Paratethys): Palaeogeographical implications from seismic sequence stratigraphy. Terra Nova 22, 12–17. https://doi.org/10.1111/j.1365-3121.2009.00910.x

Leever, K.A., Matenco, L., Garcia-Castellanos, D., Cloetingh, S.A.P.L., 2011. The evolution of the Danube gateway between Central and Eastern Paratethys (SE Europe): Insight from numerical modelling of the causes and effects of connectivity between basins and its expression in the sedimentary record. Tectonophysics 502, 175–195. https://doi.org/10.1016/j.tecto.2010.01.003

Leroy, S.A.G., Lopez-Merino, L., Tudryn, A., Chalié, F., Gasse, F., 2014. Late Pleistocene and Holocene palaeoenvironments in and around the middle Caspian basin as reconstructed from a deep-sea core. Quaternary Science Reviews 101, 91–110. https://doi.org/10.1016/j.quascirev.2014.07.011

Li, Y., Bhattacharya, J.P., 2013. Facies-Architecture Study of A Stepped, Forced Regressive Compound Incised Valley In the Ferron Notom Delta, Southern Central Utah, U.S.A. Journal of Sedimentary Research 83, 206–225. https://doi.org/10.2110/jsr.2013.19

Litt, T., Anselmetti, F.S., 2014. Lake Van deep drilling project PALEOVAN. Quaternary Science Reviews 104, 1–7. https://doi.org/10.1016/j.quascirev.2014.09.026

Magyar, I., Geary, D.H., 2012. Biostratigraphy in a Late Neogene

1424 Caspian-Type Lacustrine Basin: Lake Pannon, Hungary. Lacustrine
1425 sandstone reservoirs and hydrocarbon systems: AAPG Memoir 95
1426 255–264. https://doi.org/10.1306/13291392M953142
1427 Magyar, I., Radivojević, D., Sztanó, O., Synak, R., Ujszászi, K., Pócsik, M.,
1428 2013. Progradation of the paleo-Danube shelf margin across the
1429 Pannonian Basin during the Late Miocene and Early Pliocene.
1430 Global and Planetary Change 103, 168–173.
1431 https://doi.org/10.1016/j.gloplacha.2012.06.007
1432 Mandic, O., Kurecic, T., Neubauer, T.A., Harzhauser, M., 2015.
1433 Stratigraphic and palaeogeographic significance of lacustrine
1434 molluscs from the Pliocene Viviparus beds in central Croatia.
1435 Geologica Croatica 68, 179–207.
1436 https://doi.org/10.4154/gc.2015.15
1437 Marinescu, F., 1978. Stratigrafia Neogenului Superior din sectorul vestic
1438 al Bazinului Dacic (in Romanian). Editura Academiei Republicii
1439 Socialiste România, Bucharest, 158.
1440 Marinescu, F., Papaianopol, I., 1995. Chronostratigraphie und
1441 Neostratotypen: PL1 Dacien (in German). Editura Academiei
1442 Române, Bucharest, 536.
1443 Matenco, L., Bertotti, G., 2000. Tertiary tectonic evolution of the external
1444 East Carpathians (Romania). Tectonophysics 316, 255–286.
1445 https://doi.org/10.1016/S0040-1951(99)00261-9
1446 Matenco, L., Krézsek, C., Merten, S., Schmid, S., Cloetingh, S., Andriessen,
1447 P., 2010. Characteristics of collisional orogens with low
1448 topographic build-up: An example from the Carpathians. Terra
1449 Nova 22, 155–165. https://doi.org/10.1111/j.1365-
1450 3121.2010.00931.x
1451 Matoshko, A., Matoshko, A., de Leeuw, A., Stoica, M., 2016. Facies
1452 analysis of the Balta Formation: Evidence for a large late Miocene
1453 fluvio-deltaic system in the East Carpathian Foreland.

1454 Sedimentary Geology 343, 165–189.
1455 https://doi.org/10.1016/j.sedgeo.2016.08.004
1456 Maynard, J.R., McAllister, N., Ardic, C., 2012. Source to Sink Assessment
1457 of Oligocene to Pleistocene Sediment Supply in the Black Sea.
1458 GCSSEPM Conf. Houston Trans. 32, 664–700.
1459 Miall, A.D., 2006. The Geology of Fluvial Deposits. Sedimentary Facies,
1460 Basin Analysis, and Petroleum Geology. Springer, Heidelberg, 332.
1461 Motas, I., Bandrabur, T., Ghenea, C. Sandulescu, M., 1966. Geological
1462 map, Scale 1:200.000, sheet 36 Ploiesti. Geological Institute of
1463 Romania, Bucharest.
1464 Mulder, T., Syvitski, J.P.M., Migeon, S., Faugeres, J.C., Savoye, B., 2003.
1465 Marine hyperpycnal flows: Initiation, behavior and related
1466 deposits. A review. Marine and Petroleum Geology 20, 861–882.
1467 https://doi.org/10.1016/j.marpetgeo.2003.01.003
1468 Müller, J., Oberhänsli, H., Melles, M., Schwab, M., Rachold, V., Hubberten,
1469 H.-W., 2001. Late Pliocene sedimentation in Lake Baikal:
1470 Implications for climatic and tectonic change in SE Siberia.
1471 Palaeogeography, Palaeoclimatology, Palaeoecology 174, 305–
1472 326. https://doi.org/10.1016/S0031-0182(01)00320-0
1473 Murakoshi, N., Masuda, F., 1992. Estuarine, barrier-island to strand-
1474 plain sequence and related ravinement surface developed during
1475 the last interglacial in the Paleo-Tokyo Bay, Japan. Sedimentary
1476 Geology 80, 167–184. https://doi.org/10.1016/0037-
1477 0738(92)90039-T
1478 Necea, D., Fielitz, W., Matenco, L., 2005. Late Pliocene-Quaternary
1479 tectonics in the frontal part of the SE Carpathians: Insights from
1480 tectonic geomorphology. Tectonophysics 410, 137–156.
1481 https://doi.org/10.1016/j.tecto.2005.05.047
1482 Neubauer, T.A., Kroh, A., Harzhauser, M., Georgopoulou, E., Mandic, O.,
1483 2014. Synopsis of valid species-group taxa for freshwater

1484 Gastropoda recorded from the European Neogene. ZooKeys 435,
1485 1–6. https://doi.org/10.3897/zookeys.435.8193
1486 Neubauer, T.A., Harzhauser, M., Mandic, O., Kroh, A., Georgopoulou, E.,
1487 2016. Evolution, turnovers and spatial variation of the gastropod
1488 fauna of the late Miocene biodiversity hotspot Lake Pannon.
1489 Palaeogeography, Palaeoclimatology, Palaeoecology 442, 84–95.
1490 https://doi.org/10.1016/j.palaeo.2015.11.016
1491 Nevesskaya, L.A., Paramonova, N.P., Babak, E. V., 1997. Key to Pliocene
1492 bivalves of southwestern Eurasia (in Russian). Izvestiya Akademii
1493 Nauk SSSR, Seriya Geologischeskaya 269, 1–267.
1494 Nevesskaya, L.A., Paramonova, N.P., Popov, S. V., 2001. History of
1495 Lymnocardiinae (Bivalvia, Cardiidae). Paleontological Journal 35,
1496 143–217.
1497 Nevesskaya, L.A., Goncharova, I.A., Ilyina, L.B., Paramonova, N.P.,
1498 Khondkarian, S.O., 2003. The Neogene Stratigraphic Scale of the
1499 Eastern Paratethys. Stratigraphy and Geological Correlation 11,
1500 105–127.
1501 Nevesskaya, L.A., Goncharova, I.A., Ilina, L.B., Popov, S. V., 2009.
1502 Evolutionary transformations of the malacofaunas in the Neogene
1503 basins of paratethys as an example of development of the
1504 ecosystems of insular type (in Russian). Journal of General
1505 Geology 70, 396–414.
1506 Nevesskaya, L.A., Popov, S. V., Goncharova, I.A., Guzhov, A. V., Janin, B.T.,
1507 Polubotko, I. V., Biakov, A.S., Gavrilova, A.S., 2013. Phanerozoic
1508 Bivalvia of Russia and surrounding countries (in Russian).
1509 Izvestiya Akademii Nauk SSSR, Seriya Geologischeskaya 294, 1–
1510 524.
1511 Nummedal, D., Swift, D.J.P., 1987. Transgressive stratigraphy at
1512 sequence-bounding unconformities: some principles derived from
1513 Holocene and Cretaceous examples. Sea level fluctuation and

coastal evolution 41, 241–260. https://doi.org/10.2110/pec.87.41.0241

Nutz, A., Schuster, M., Boës, X., Rubino, J.-L., 2017. Orbitally-driven evolution of Lake Turkana (Turkana Depression, Kenya, EARS) between 1.95 and 1.72 Ma: A sequence stratigraphy perspective. Journal of African Earth Sciences 125, 230–243. https://doi.org/10.1016/j.jafrearsci.2016.10.016

Olariu, C., Bhattacharya, J.P., 2006. Terminal Distributary Channels and Delta Front Architecture of River-Dominated Delta Systems. Journal of Sedimentary Research 76, 212–233. https://doi.org/10.2110/jsr.2006.026

Olariu, M.I., Olariu, C., 2015. Ubiquity of wave-dominated deltas in outer-shelf growth-faulted compartments. Journal of Sedimentary Research 85, 768–779. https://doi.org/10.2110/jsr.2015.51

Olariu, C., Krezsek, C., Jipa, D., 2017. The Danube River inception: Evidence for a 4 Ma continental-scale river born from segmented ParaTethys basins. Terra Nova.

Oliveira, C.M.M., Hodgson, D.M., Flint, S.S., 2009. Aseismic controls on in situ soft-sediment deformation processes and products in submarine slope deposits of the Karoo Basin, South Africa. Sedimentology 56, 1201–1225. https://doi.org/10.1111/j.1365-3091.2008.01029.x

Overeem, I., Kroonenberg, S.B., Veldkamp, A., Groenesteijn, K., Rusakov, G. V., Svitoch, A.A., 2003. Small-scale stratigraphy in a large ramp delta: Recent and Holocene sedimentation in the Volga delta, Caspian Sea. Sedimentary Geology 159, 133–157. https://doi.org/10.1016/S0037-0738(02)00256-7

Panaiotu, C.E., Vasiliev, I., Panaiotu, C.G., Krijgsman, W., Langereis, C.G., 2007. Provenance analysis as a key to orogenic exhumation: A case study from the East Carpathians (Romania). Terra Nova 19,

120–126. https://doi.org/10.1111/j.1365-3121.2006.00726.x

Panin, N., Jipa, D., 2002. Danube River Sediment Input and its Interaction with the North-western Black Sea. Estuarine, Coastal and Shelf Science 54, 551–562. https://doi.org/10.1006

Piller, W.E., Harzhauser, M., Mandic, O., 2007. Miocene Central Paratethys stratigraphy – current status and future directions. Stratigraphy 4, 151–168.

Popov, S. V., Shcherba, I.G., Ilyina, L.B., Nevesskaya, L.A., Paramonova, N.P., Khondkarian, S.O., Magyar, I., 2006. Late Miocene to Pliocene palaeogeography of the Paratethys and its relation to the Mediterranean. Palaeogeography, Palaeoclimatology, Palaeoecology 238, 91–106.

Popa, O.P.., Kelemen, B.S.., Iorgu, E.I.., Popa, L.., 2009. Contributions to the knowledge of the present Limnocardiidae fauna (Mollusca, Bivalvia) from Romania. Travaux du Muséum National d'Histoire Naturelle «Grigore Antipa» LII, 7–15. https://doi.org/10.1016/j.palaeo.2006.03.020

Postma, G., 1990. Depositional Architecture and Facies of River and Fan Deltas: A Synthesis. Special Publication of the International Association of Sedimentologists 10, 13–27. https://doi.org/10.1002/9781444303858.ch2

Rögl, F., 1998. Palaeogeographic Considerations for Mediterranean and Paratethys Seaways (Oligocene to Miocene). Annalen des Naturhistorischen Museums in Wien 99, 279–310.

Ross, D.A., 1978. Black Sea Stratigraphy. Deep Sea Drilling Project Initial Reports 42, 17–26.

Sacchi, M., Müller, P., 2004. Orbital cyclicity and astronomical calibration of the Upper Miocene continental succession cored at Iharosber ny-I well site, western Pannonian basin, Hungary. SEPM Special Publication 81, 275–294.

1574 Sanders, C.A.E., Andriessen, P.A.M., Cloetingh, S.A.P.L., 1999. Life cycle of
1575 the East Carpathian orogen: Erosion history of a doubly vergent
1576 critical wedge assessed by fission track thermochronology.
1577 Journal of Geophysical Research 104, 29095–29112.
1578 https://doi.org/10.1029/1998JB900046
1579 Scarponi, D., Kaufman, D., Amorosi, A., Kowalewski, M., 2013. Sequence
1580 stratigraphy and the resolution of the fossil record. Geology 41,
1581 239–242. https://doi.org/10.1130/G33849.1
1582 Schmid, S.M., Bernoulli, D., Fugenschuh, B., Matenco, L., Schefer, S.,
1583 Schuster, R., Tischler, M., Ustaszewski, K., 2008. The Alpine-
1584 Carpathian-Dinaridic orogenic system: Correlation and evolution
1585 of tectonic units. Swiss Journal of Geosciences 101, 139–183.
1586 https://doi.org/10.1007/s00015-008-1247-3
1587 Snel, E., Mărunţeanu, M., Macaleţ, R., Meulenkamp, J.E., van Vugt, N.,
1588 2006. Late Miocene to Early Pliocene chronostratigraphic
1589 framework for the Dacic Basin, Romania. Palaeogeography,
1590 Palaeoclimatology, Palaeoecology 238, 107–124.
1591 https://doi.org/10.1016/j.palaeo.2006.03.021
1592 Starek, D., Pipík, R., Hagarová, I., 2010. Meiofauna, trace metals, TOC,
1593 sedimentology, and oxygen availability in the Late Miocene
1594 sublittoral deposits of Lake Pannon. Facies 56, 369–384.
1595 https://doi.org/10.1007/s10347-009-0208-2
1596 Stoica, M., Lazăr, I., Krijgsman, W., Vasiliev, I., Jipa, D., Floroiu, A., 2013.
1597 Paleoenvironmental evolution of the East Carpathian foredeep
1598 during the late Miocene-early Pliocene (Dacian Basin; Romania).
1599 Global and Planetary Change 103, 135–148.
1600 https://doi.org/10.1016/j.gloplacha.2012.04.004
1601 Sturm, M., Matter, A., 1978. Turbidites and varves in Lake Brienz
1602 (Switzerland): deposition of clastic detritus by density currents,
1603 in: Matter, A., Tucker, M.E. (Eds.), Modern and Ancient Lake

1604 Sediments, Special Publication 2, International Association of
1605 Sedimentologists. Wiley Blackwell, Oxford, pp. 147–168.
1606 Sztanó, O., Magyar, I., Szónoky, M., Lantos, M., Müller, P., Lenkey, L.,
1607 Katona, L., Csillag, G., 2013. Tihany Formation in the surroundings
1608 of Lake Balaton: type locality, depositional setting and
1609 stratigraphy (in Hungarian). Földtani Közlöny 143, 73–98.
1610 Tărăpoancă, M., Bertotti, G., Matenco, L., Dinu, C., Cloetingh, S.A.P.L.,
1611 2003. Architecture of the Focşani Depression: A 13 km deep basin
1612 in the Carpathians bend zone (Romania). Tectonics 22, 1-7.
1613 https://doi.org/10.1029/2002TC001486
1614 Ter Borgh, M., Stoica, M., Donselaar, M.E., Matenco, L., Krijgsman, W.,
1615 2014. Miocene connectivity between the Central and Eastern
1616 Paratethys: Constraints from the western Dacian Basin.
1617 Palaeogeography, Palaeoclimatology, Palaeoecology 412, 45–67.
1618 https://doi.org/10.1016/j.palaeo.2014.07.016
1619 Vakarcs, G., Vail, P.R., Tari, G., Pogácsás, G., Mattick, R.E., Szabó, A., 1994.
1620 Third-order Middle Miocene-Early Pliocene depositional
1621 sequences in the prograding delta complex of the Pannonian
1622 Basin. Tectonophysics 240, 81–106.
1623 https://doi.org/10.1016/0040-1951(94)90265-8
1624 Van Baak, C.G.C., Mandic, O., Lazar, I., Stoica, M., Krijgsman, W., 2015.
1625 The Slanicul de Buzau section, a unit stratotype for the Romanian
1626 stage of the Dacian Basin (Plio-Pleistocene, Eastern Paratethys).
1627 Palaeogeography, Palaeoclimatology, Palaeoecology 440, 594–
1628 613. https://doi.org/10.1016/j.palaeo.2015.09.022
1629 Vasiliev, I., Krijgsman, W., Langereis, C.G., Panaiotu, C.E., Maţenco, L.,
1630 Bertotti, G., 2004. Towards an astrochronological framework for
1631 the eastern Paratethys Mio-Pliocene sedimentary sequences of the
1632 Focşani basin (Romania). Earth and Planetary Science Letters 227,
1633 231–247. https://doi.org/10.1016/j.epsl.2004.09.012

1634 Vasiliev, I., Krijgsman, W., Stoica, M., Langereis, C.G., 2005. Mio-Pliocene
1635 magnetostratigraphy in the southern Carpathian foredeep and
1636 Mediterranean-Paratethys correlations. Terra Nova 17, 376–384.
1637 https://doi.org/10.1111/j.1365-3121.2005.00624.x
1638 Vasiliev, I., Maţenco, L., Krijgsman, W., 2009. The syn- and post-
1639 collisional evolution of the Romanian Carpathian foredeep: New
1640 constraints from anisotropy of magnetic susceptibility and
1641 paleostress analyses. Tectonophysics 473, 457–465.
1642 https://doi.org/10.1016/j.tecto.2009.04.002
1643 Vincent, S.J., Morton, A.C., Carter, A., Gibbs, S., Teimuraz, G., 2007.
1644 Oligocene uplift of the Western Greater Caucasus : an effect of
1645 initial Arabia – Eurasia collision. Terra Nova 19, 160–166.
1646 https://doi.org/10.1111/j.1365-3121.2007.00731.x
1647 Vincent, S.J., Davies, C.E., Richards, K., Aliyeva, E., 2010. Contrasting
1648 Pliocene fluvial depositional systems within the rapidly subsiding
1649 South Caspian Basin; a case study of the palaeo-Volga and palaeo-
1650 Kura river systems in the Surakhany Suite, Upper Productive
1651 Series, onshore Azerbaijan. Marine and Petroleum Geology 27.
1652 2079-2106. https://doi.org/10.1016/j.marpetgeo.2010.09.007
1653 Vincent, S.J., Braham, W., Lavrishchev, V.A., Maynard, J.R., Harland, M.,
1654 2016. The formation and inversion of the western Greater
1655 Caucasus Basin and the uplift of the western Greater Caucasus:
1656 Implications for the wider Black Sea region. Tectonics 35, 2948–
1657 2962. https://doi.org/10.1002/2016TC004204
1658 Wagner, B., Wilke, T., Krastel, S., Zanchetta, G., Sulpizio, R., Reicherter,
1659 K., Leng, M.J., Grazhdani, A., Trajanovski, S., Francke, A., Lindhorst,
1660 K., Levkov, Z., Cvetkoska, A., Reed, J.M., Zhang, X., Lacey, J.H.,
1661 Wonik, T., Baumgarten, H., Vogel, H., 2014. The SCOPSCO drilling
1662 project recovers more than 1.2 million years of history from Lake
1663 Ohrid, Scientific Drilling, 19-29. https://doi.org/10.5194/sd-17-

19-2014

Weimer, R., 1988. Record of relative sea-level changes, Cretaceous of Western Interior, USA. SEPM Special Publication 42, 285–288.

Wenz, W., 1942. Die Mollusken des Pliozäns der rumänischen Erdöl-Gebiete als Leitversteinerungen für die Aufschluß-Arbeiten (in German). Senckenbergiana 24, 1–293.

Wesselingh, F.P., Kaandorp, R.J.G., Vonhof, H.B., Räsänen, M.E., Renema, W., Gingras, M., 2006. The nature of aquatic landscapes in the Miocene of western Amazonia: An integrated palaeontological and geochemical approach. Scripta Geologica 363–393.

Wilke, T., Wagner, B., Van Bocxlaer, B., Albrecht, C., Ariztegui, D., Delicado, D., Francke, A., Harzhauser, M., Hauffe, T., Holtvoeth, J., Just, J., Leng, M.J., Levkov, Z., Penkman, K., Sadori, L., Skinner, A., Stelbrink, B., Vogel, H., Wesselingh, F., Wonik, T., 2016. Scientific drilling projects in ancient lakes: Integrating geological and biological histories. Global and Planetary Change 143, 118–151. https://doi.org/10.1016/j.gloplacha.2016.05.005

Wortel, M.J.R., Spakman, W., 2000. Subduction and Slab Detachment in the Mediterranean-Carpathian Region. Science 290, 1910–1917.

Yanina, T.A., 2014. The Ponto-Caspian region: Environmental consequences of climate change during the Late Pleistocene. Quaternary International 345, 88–99. https://doi.org/10.1016/j.quaint.2014.01.045

Figure captions

Fig. 1: a) Palaeogeographical map of the Paratethyan Basins during the Early Pliocene (adapted from Popov et al., 2006). b) Enlarged palaeogeographical map of the semi-isolated Dacian Basin during the mid-Pliocene, with associated water connections to adjacent basins and drainage systems (adapted from Popov et al., 2006). Studied section marked by a red star.

Fig. 2: a) International stratigraphic nomenclature during the Plio-Pleistocene (Cohen et al., 2013 updated), correlated with the regional stages of the Dacian Basin (work realised by: 1) Krijgsman et al., 2010; 2) Vasiliev et al., 2005 and 3) van Baak et al., 2015. b) Detailed geological map of the Eastern Carpathians foreland basin affected by large-scale folding (adapted from Dumitrescu et al., 1970; Motas et al., 1966; van Baak et al., 2015). Slănicul de Buzău section mark by a red line. c) Enlarged geological map of the studied section, running through the top of a plunging anticline. Studied Dacian interval marked by a red line.

Fig. 3: a) Sedimentological log of the Slănicul de Buzău section with measured magnetostratigraphic time frame. In orange, stratigraphic position of the detailed sedimentological logs of some of the parasequences shown in figure 14. In red, stratigraphic position of the clayish and sandy parasequences illustrated in figure 15 and 16. b) Relative water-level curve of the Dacian interval based on facies depth ranks, as explained in Table 1, and interpreted low-order sequences (dark gray) and high-order sequences (light gray).

Fig. 4: Stereonet projection of the measured bedding planes along the Slănicul de Buzău section and their poles in blue. Deduced fold axis running and its pole in red. Corrected pole of the fold axis in green.

Fig. 5: Cardiids (1-26), unionids (27-28), dreissenids (29-32) and viviparids (33-34) present in the Dacian interval of the Slănicul de Buzău section. 1. *Euxinicardium olivetum*; 2. *Tauricardium olteniae*; 3. *Dacicardium rumanum*; 4. *Phyllocardium planum*; 5. *Pontalmyra tohanensis*; 6. *Pontalmyra conversa*; 7. *Pseudocatillus dacianus*; 8. *Chartoconcha bayerni*; 9. *Chartoconcha ovata*; 10. *Chartoconcha rumana*; 11. *Caladacna steindacheri*; 12. *Stylodacna heberti*; 13. *Pachydacna* (*Parapachydacna*) *orbiculata*; 14. *Pachydacna* (*Parapachydacna*) *cobalcescui*; 15. *Pachydacna* (*Parapachydacna*) *serena*; 16. *Prosodacnomya sturi*; 17. *Prosodacna semisulacata*; 18. *Prosodacna minima*; 19. *Prosodacna obovata*; 20. *Psilodon haueri*; 21. *Psilodon munieri*; 22-23. *Psilodon neumayri*; 24. *Zamphiridacna motasi*; 25. *Zamphiridacna orientalis*; 26. *Zamphiridacna zamphiri*; 27. *Rumanunio rumanus*; 28. *Hyriopsis krejcii*; 29. *Dreissena polymorpha*; 30. *Dreissena rimestiensis*; 31. *Dreissena rostriformis*; 32. *Andrusoviconcha botenica*; 33. *Viviparus argosiensis*; 34. *Viviparus rumanus*.

Fig. 6: Most common ostracods present in the Lower Dacian along the Slănicul de Buzău section (Part I, 1-22). 1. *Amplocypris dorsobrevis* (Sakac), 2. *Amplocypris dorsobrevis* (Sakac), pyritized internal cast; 3-8. *Pontoniella* ex. gr. *quadrata* (Krstić); 9-10. *Candona (Camptocypria)* ex. gr. *balcanica* (Zalányi); 11-12. *Candona (Caspiocypris) alta* (Zalányi); 13. *Bakunella dorsoarcuata* (Zalányi), bad preserved specimen; 14-15. F*abaeoformiscandona* sp.; 16-17. *Candona (Camptocypria)* sp.; 18. *Tyrrhenocythere* sp., fragment; 19. *Loxoconcha babazananica* (Livental); 20. *Amnicythere andrusovi* (Livental); 21-22. *Amnicythere* ex. gr. *cymbula* (Livental).

Fig. 7: Most common ostracods present in the Lower Dacian along the Slănicul de Buzău section (Part II, 1-25) and fish teeth (26-27). 1-8. *Cytherissa bogatschovi* (Livental); 9-14. *Cyprideis* ex. gr. *torosa* (Jones); 15-20. *Cyprideis* ex. gr. *torosa* (Jones); 21-25. Microgastropods: 21-24. *Melanoides* sp.; 25. *Pyrgula* sp.; 26-27. *Gobiidae* fish teeth.

Fig. 8: Most common ostracod present in the Upper Dacian along the Slănicul de Buzău section (Part I, 1-22). 1-6. *Candona (Caspiocypris) alta* (Zalányi); 7. *Candona (Caspiocypris) ornata* Hanganu; 8-9. *Candona* ex. gr. *neglecta* (G. O. Sars); 10-13. *Candona (Camptocypria)* ex. gr. *balcanica* (Zalányi); 14-15. *Scottia kempfi* (Hanganu); 16-17. *Cyclocypris laevis* (O. F. Müller); 18. *Amplocypris* sp.; 19-22. *Pontoniella* ex. gr. *quadrata* (Krstić).

Fig. 9: Most common ostracods present along the Slănicul de Buzău section in the Upper Dacian (Part II, 1-22). 1-8. *Cyprideis* ex. gr. *torosa* (Jones); 9-18. *Cytherissa bogatschovi* (Livental); 19-22. *Loxoconcha* ex. gr. *schweyeri* (Suzin); 23-24. *Ilyocypris bradyi* (G. O. Sars).

Fig. 10: Pictures of the different lithofacies identified along the section (Part I). a) Organic-rich clays Cm. b) Massive mudstone Fm. c) Laminated mudstone Fl. d) Lenticular mudstone Fs. e) Massive sandstone Sm. f) Low-angle cross-stratified sandstone Sl. g) Horizontally laminated sandstone.

Fig. 11: Pictures of the different lithofacies identified along the section (Part II). a) Current rippled sandstone Sc. b) Climbing rippled sandstone Sr. c) Sigmoidal cross-stratified sandstone Ss. d) Trough cross-stratified sandstone St. e) Grayish shelly sandstone Sfg. f) Reddish shell-rich sandstone Sfr.

Fig. 12: Palaeocurrent directions measured along the studied section. a) Direction of progradation measured for the pro-delta sediments. b) Direction of progradation measured for delta-front sediments. c) Direction of progradation measured for delta-top sediments. d) Direction of progradation measured for the entire Dacian stage interval.

Fig. 13: Thin-section photograph of a sigmoidal cross-stratified sandstone realised a) under polarized light and b) under polarized and analysed light. Thin-section photograph of an oxidized shell-rich sandstone c) under polarized light and d) under polarized and analysed light.

Fig. 14: Sedimentological logs of some of the most representative regressive parasequences observed along the studied section.

Fig. 15: Photograph and corresponding sedimentological log from a succession of several thick clayish parasequences. Illustrations of some typical distal sedimentary deposits. a) Hyperpycnal flow deposit. b) Convolute bedding. c) Small-scale sedimentary structures in sandstone.

Fig. 16: Photograph and corresponding sedimentological log from a succession of several thin sandy parasequences. Illustrations of some typical proximal sedimentary deposits. a) Frequent gravity current deposits. b) Meter-thick erosive mouth bar deposit. c) Indurated and burrowed coastal-plain mire deposit.

Fig. 17: Age model proposed for the Slănicul de Buzău section by correlating the measured magnetostratigraphic time frame with the international magnetostratigraphic timescale from 4.8 to 4.0 Ma (Gradstein et al., 2012). Plotting of the selected bandpass filters again the Milankovitch astronomical target curves: eccentricity, obliquity and precession (Laskar et al., 2011).

Fig. 18: Sedimentation rates calculated along the studied section. Comparison with the low-order sequences (dark gray) and the high-order sequences (light gray).

Tab. 1: Facies depth ranks used to create the relative water-level curve of the studied section.

Tab. 2: Mollusc faunas distribution according to their stratigraphic position along the along the studied section. The green frame indicates the stratigraphic position of the transition between the marker species for the Lower Dacian (dark gray) and the marker species for the Upper Dacian (light gray), used to place the boundary between the Lower and Upper Dacian regional substages.

Tab. 3: Description of the main lithofacies characteristics and associated sedimentary processes identified along the studied section.

Tab. 4: Mollusc faunas distribution according to their depositional environment. In dark red, the marker species for brackish-waters environments. In light red, the species found mostly in brackish-

waters environments. In dark green, the marker species for fresh-waters environments. In light green, the species found mostly in fresh-waters environments.

Figure 1

Click here to download high resolution image

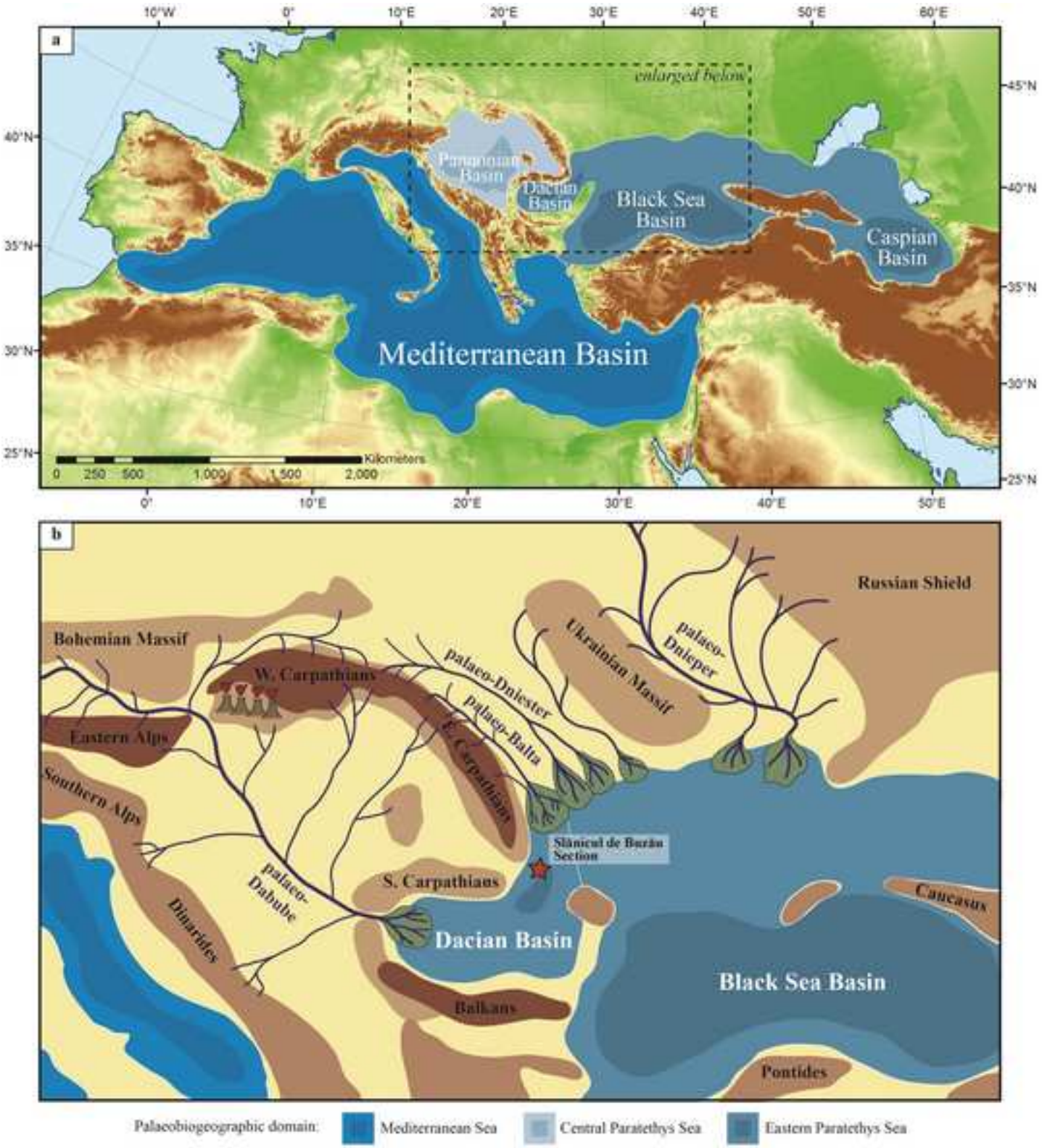

Figure 2

Click here to download high resolution image

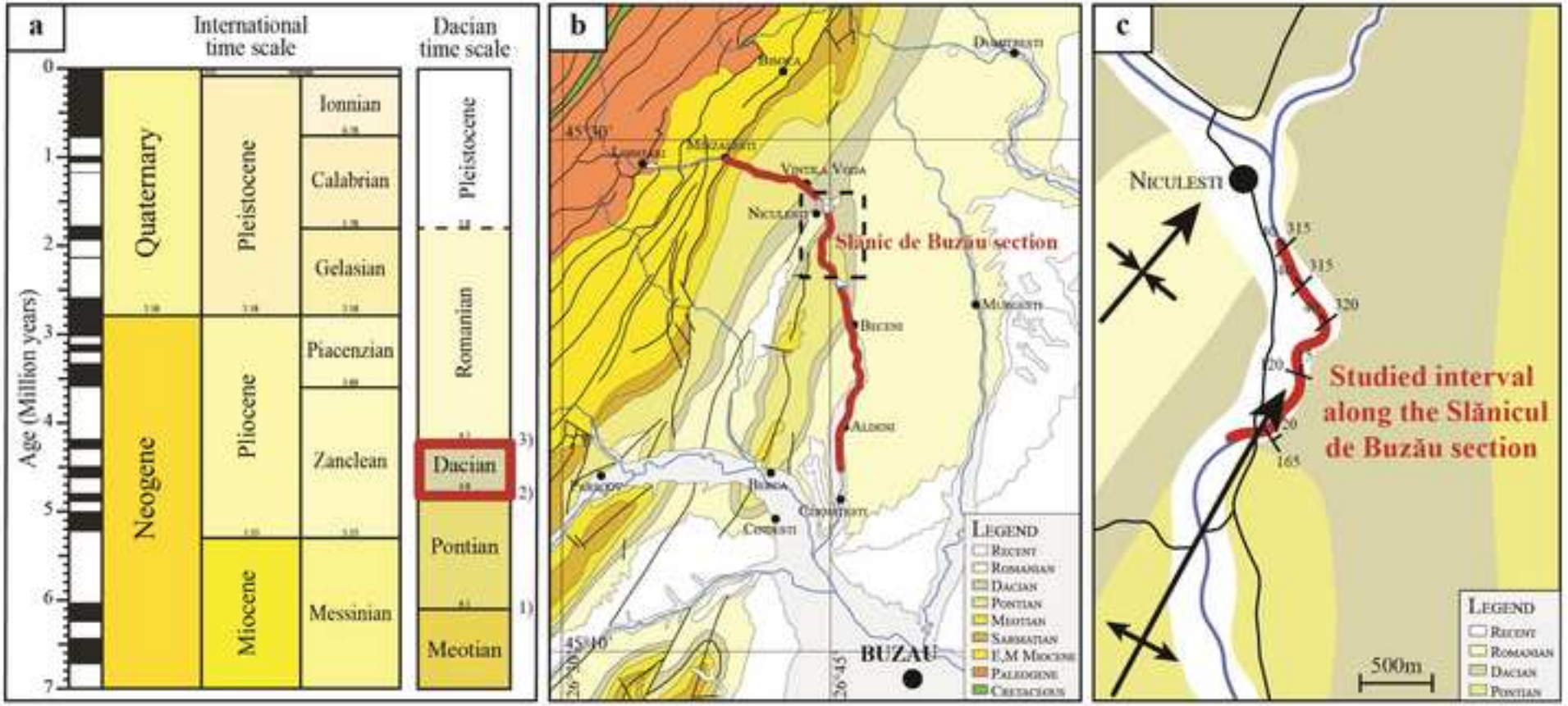

Figure 3

Click here to download high resolution image

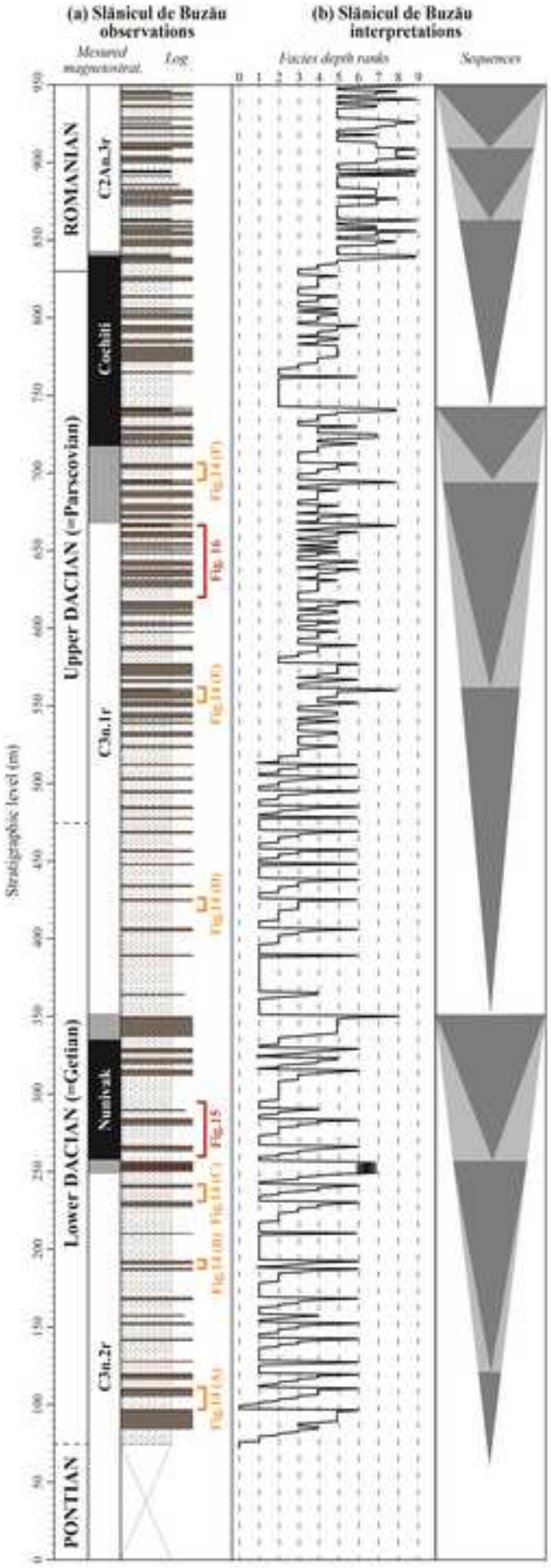

Figure 4

Click here to download high resolution image

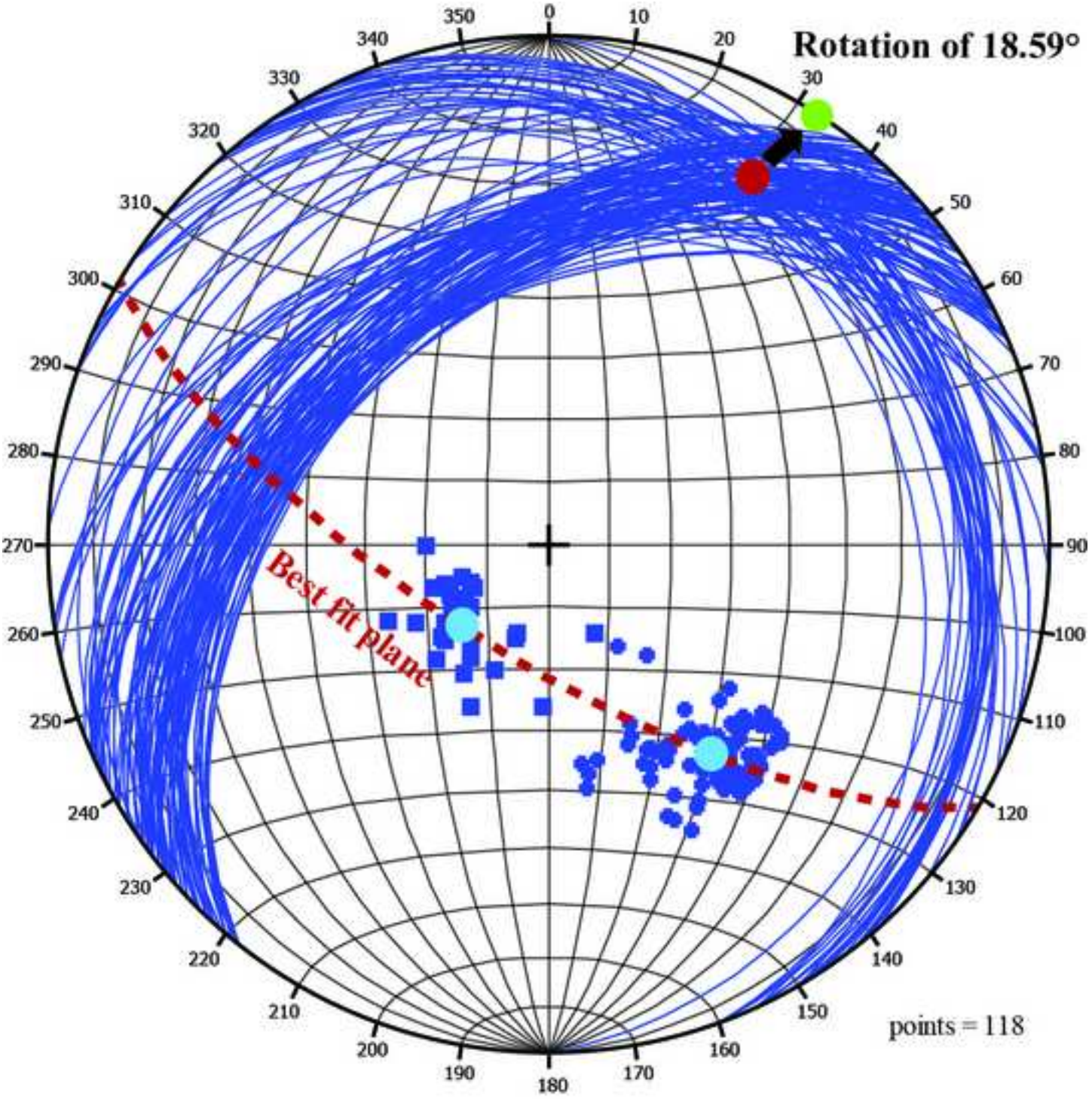

Bedding planes

Poles of the bedding planes

Poles of the two average bedding planes: - average plane 1 (azimuth, dip): 321.92°/43.81°
- average plane 2 (azimuth, dip): 47.67°/18.71°

Fold axis plane (longitudinal orientation/best fit plane - dip azimuth, dip): 211.16°/71.41°

Pole of the fold axis (plunge azimuth, plunge): 31.16°/18.59°

Corrected pole of the fold axis (plunge azimuth, plunge): 31.16°/0.00°

Figure 5

Click here to download high resolution image

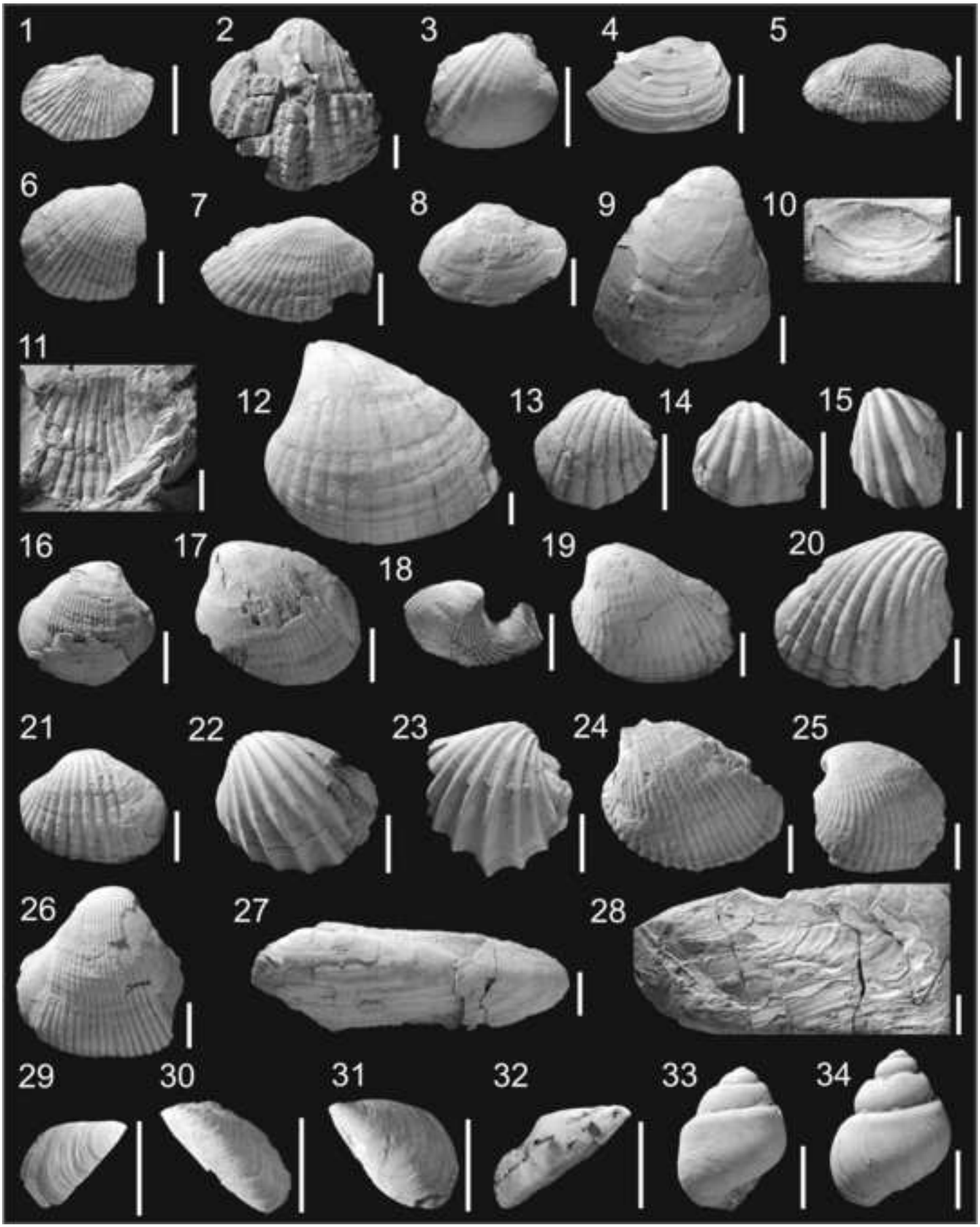

Figure 6

Click here to download high resolution image

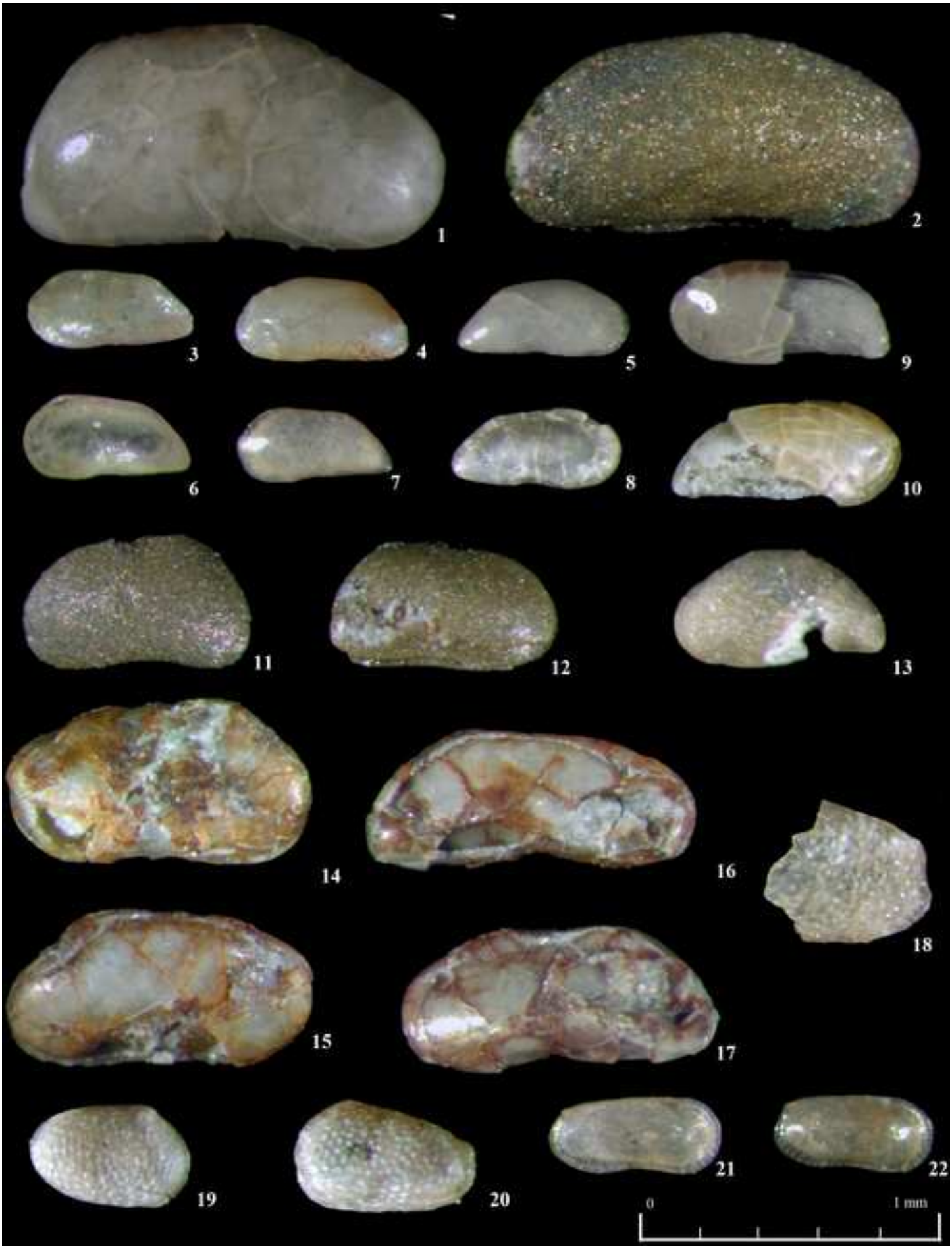

Figure 7

Click here to download high resolution image

Figure 8

Click here to download high resolution image

Figure 9

Click here to download high resolution image

Figure 10

Click here to download high resolution image

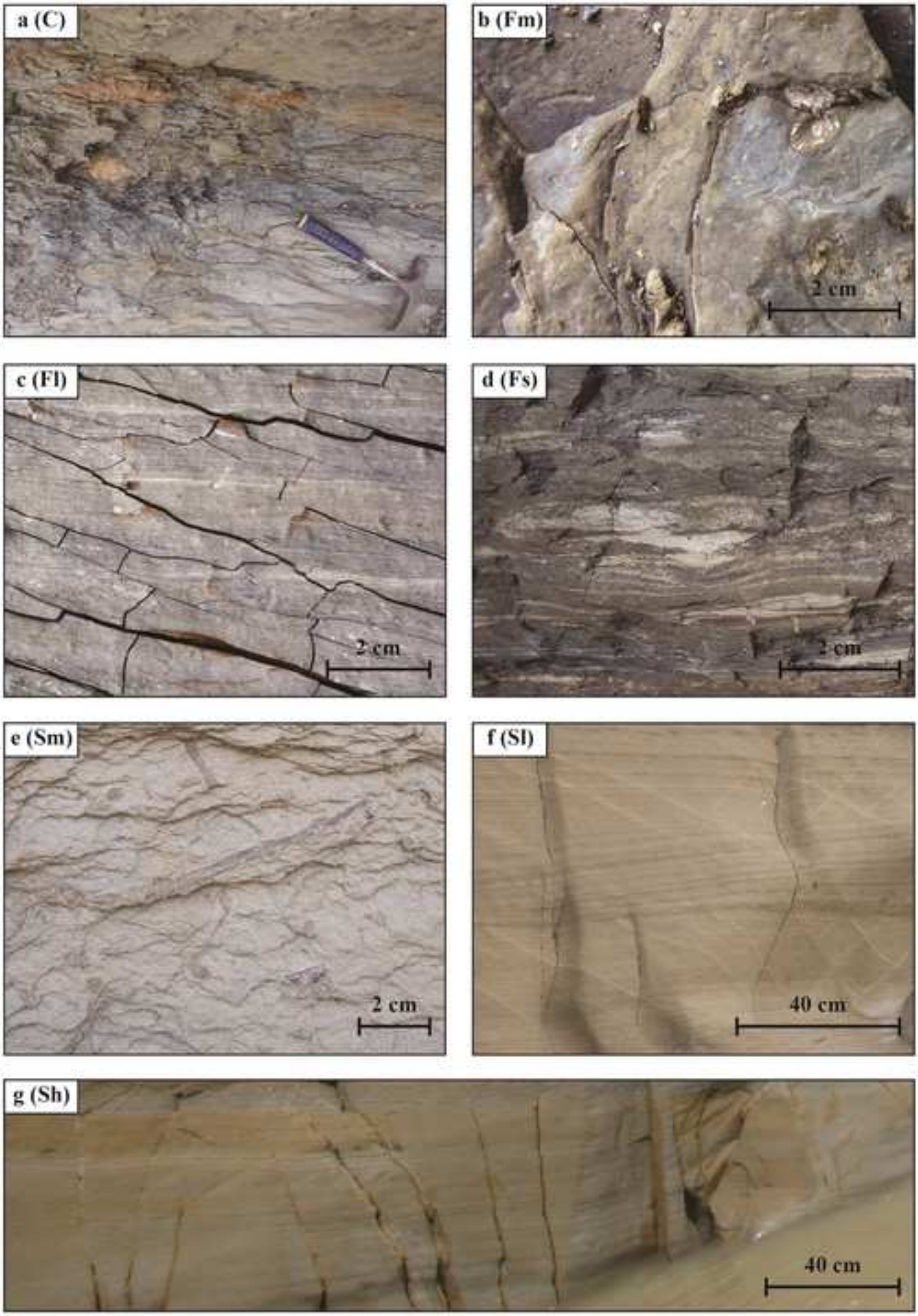

Figure 11

Click here to download high resolution image

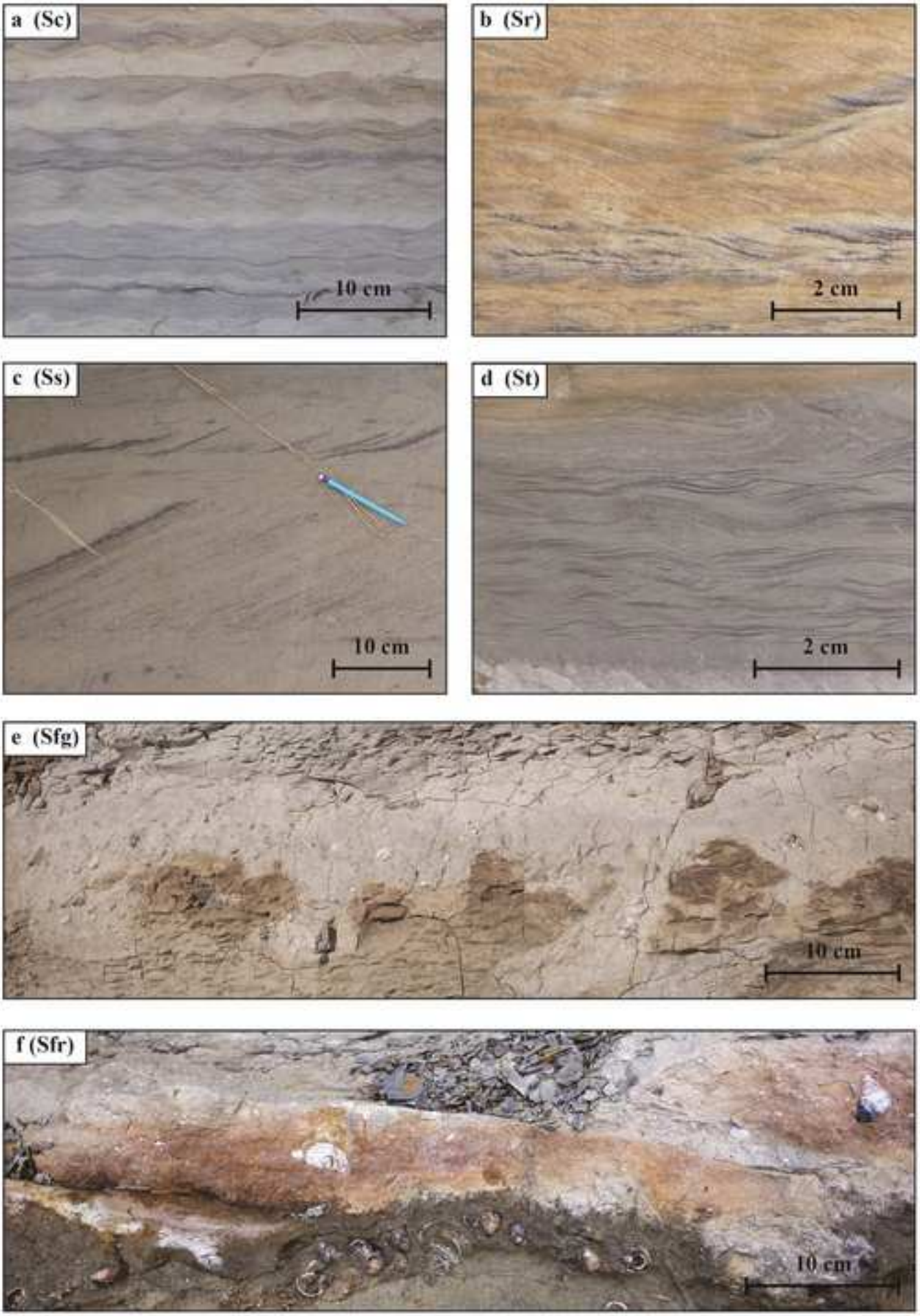

Figure 12

Click here to download high resolution image

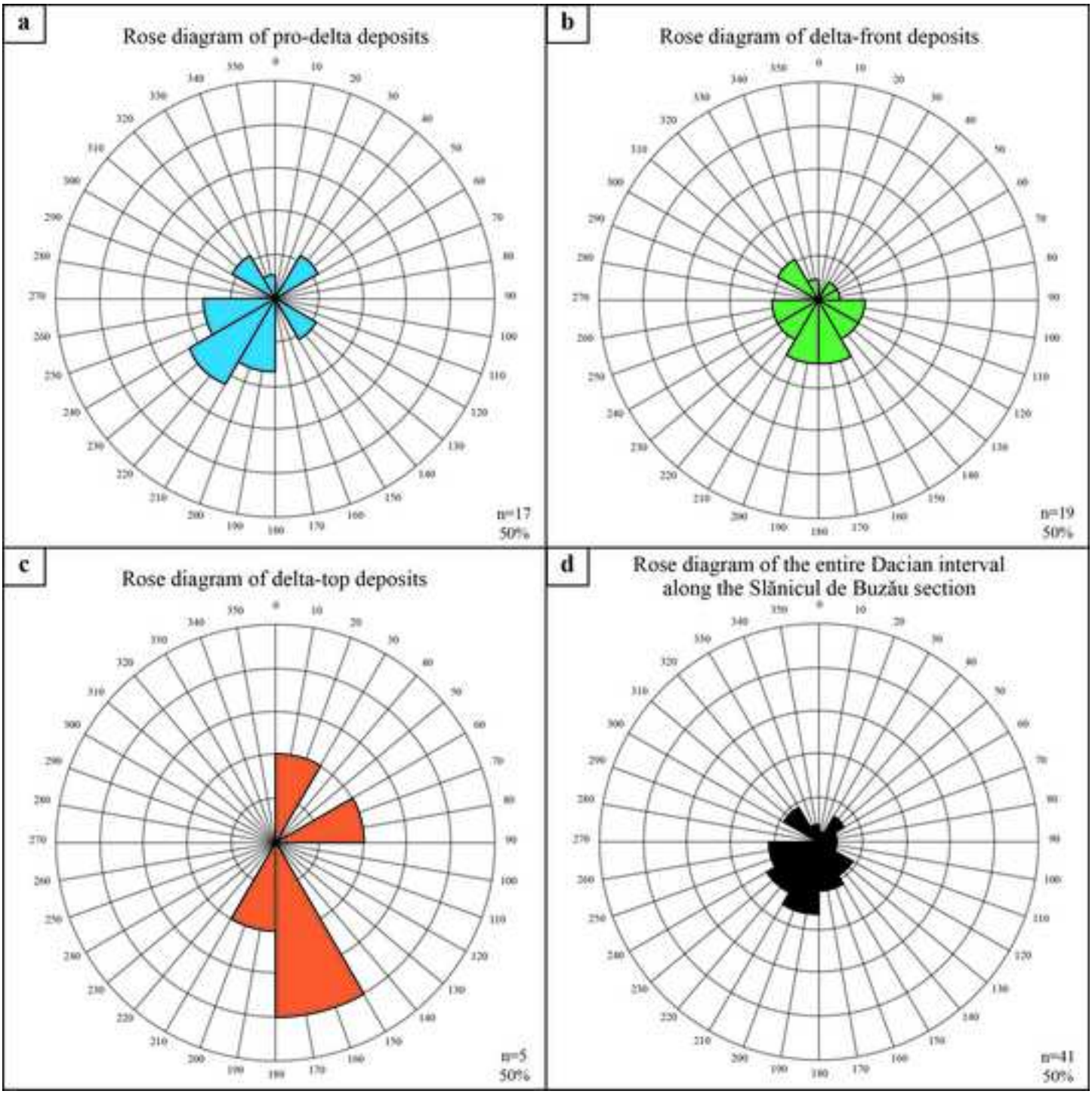

Figure 13

Click here to download high resolution image

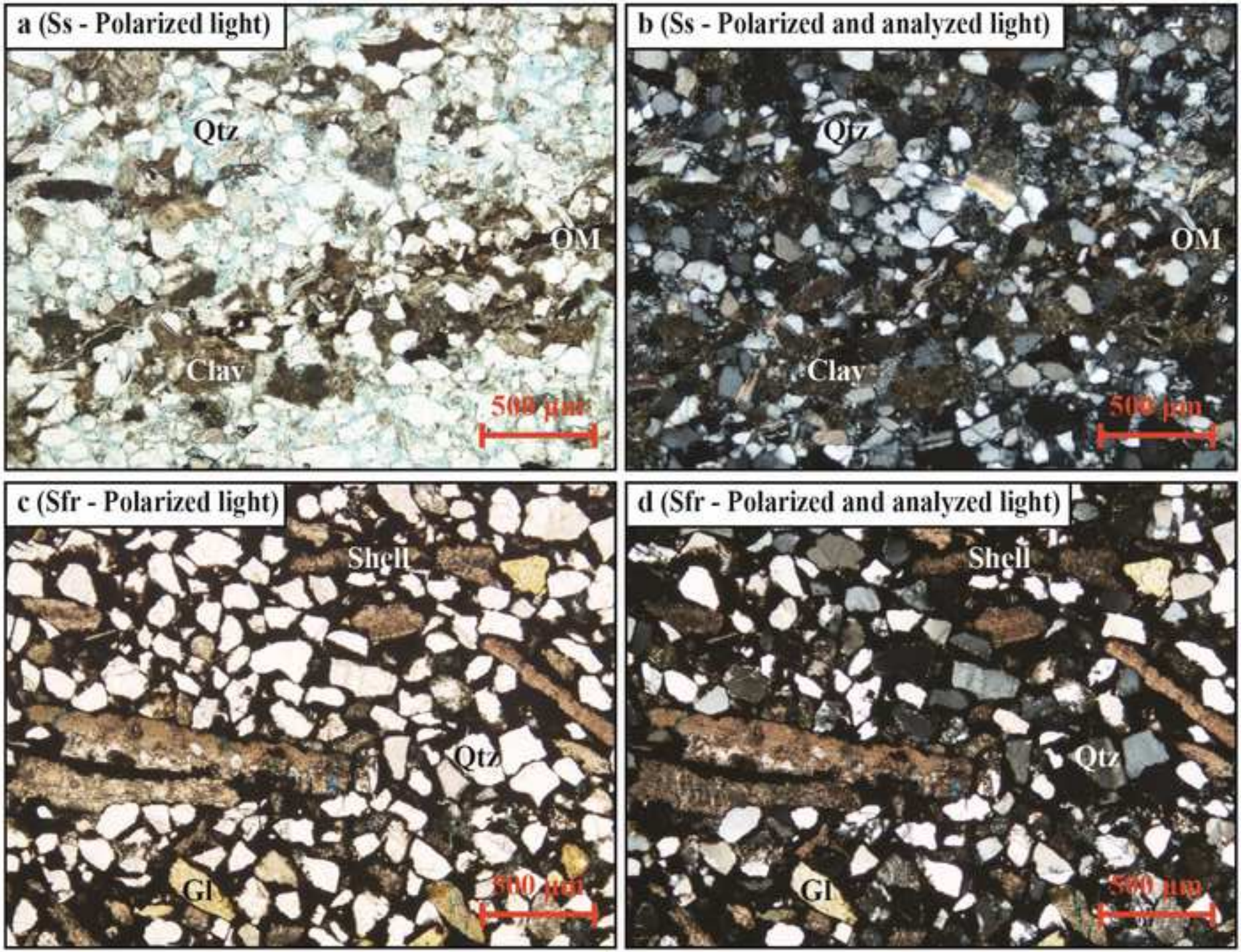

Figure 14

Click here to download high resolution image

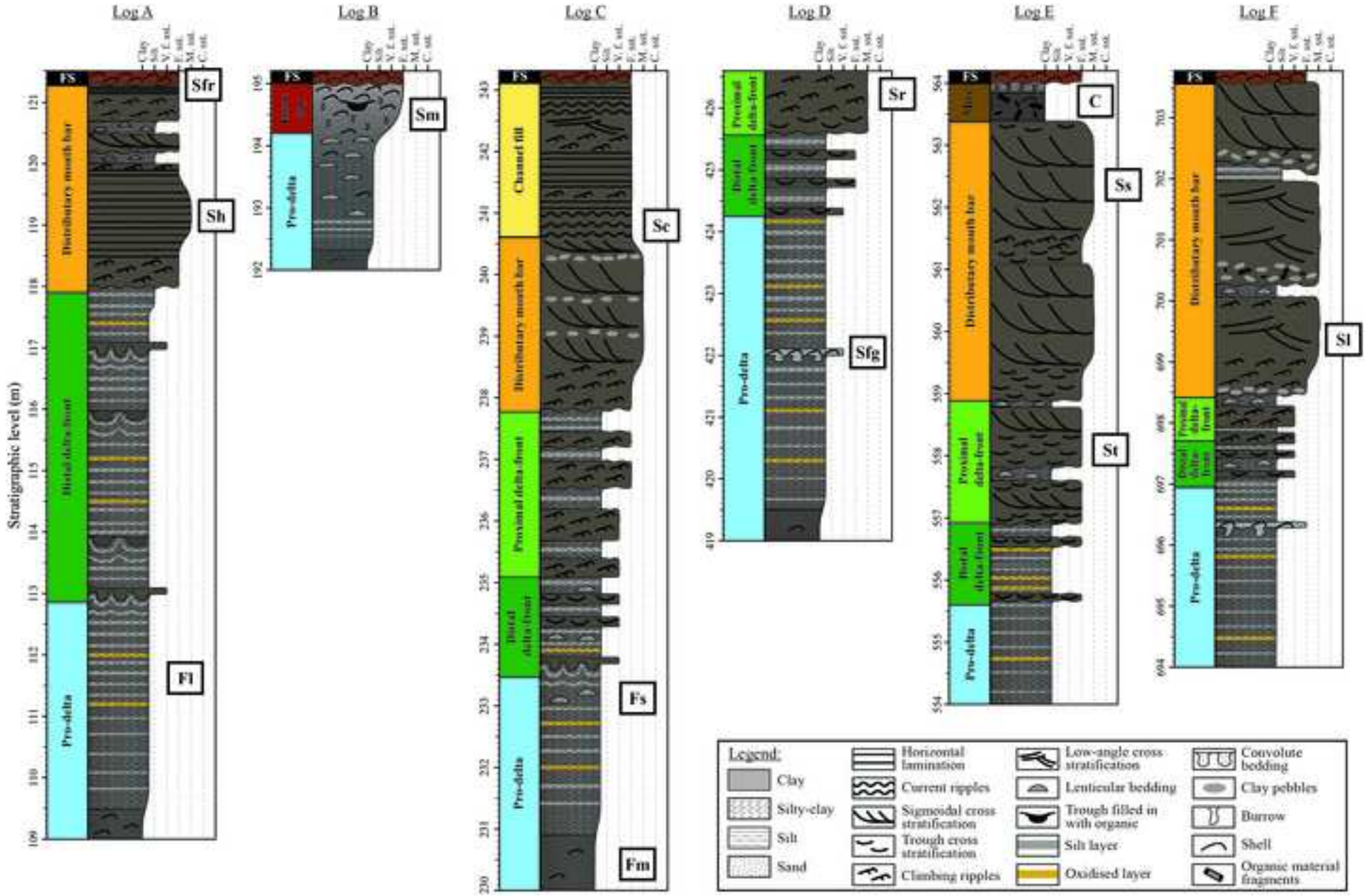

Figure 15

Click here to download high resolution image

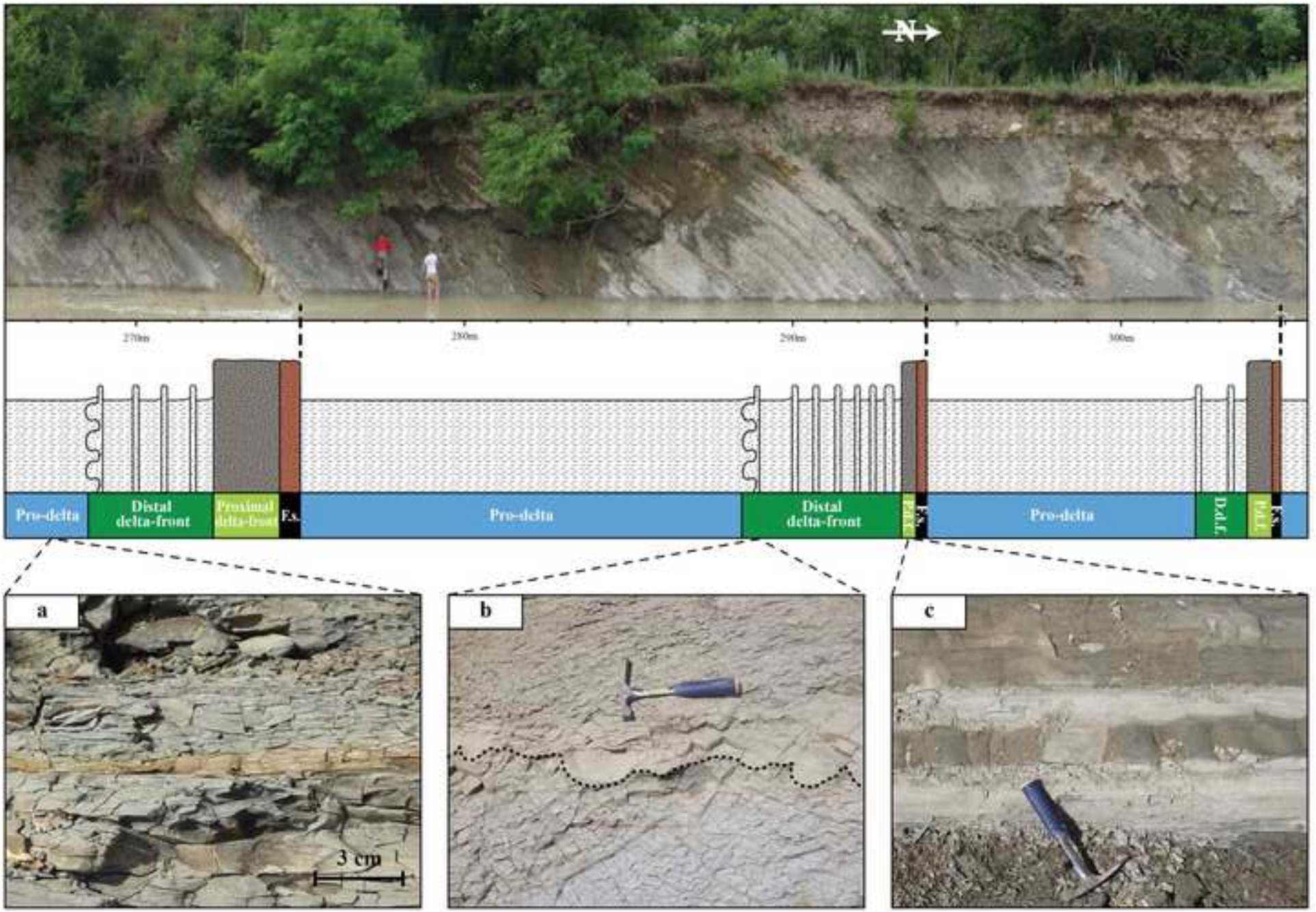

Figure 16

Click here to download high resolution image

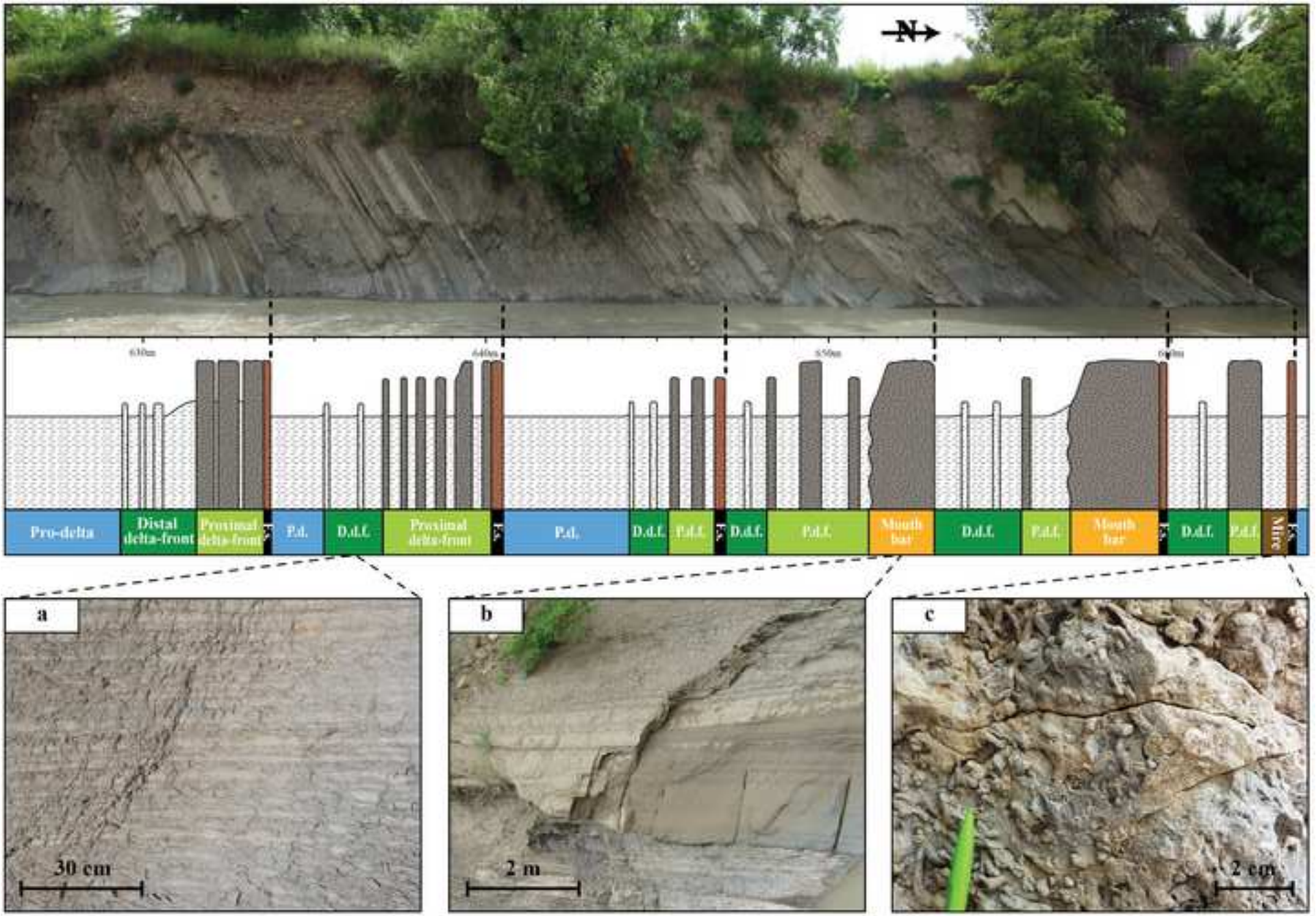

Figure 17

Click here to download high resolution image

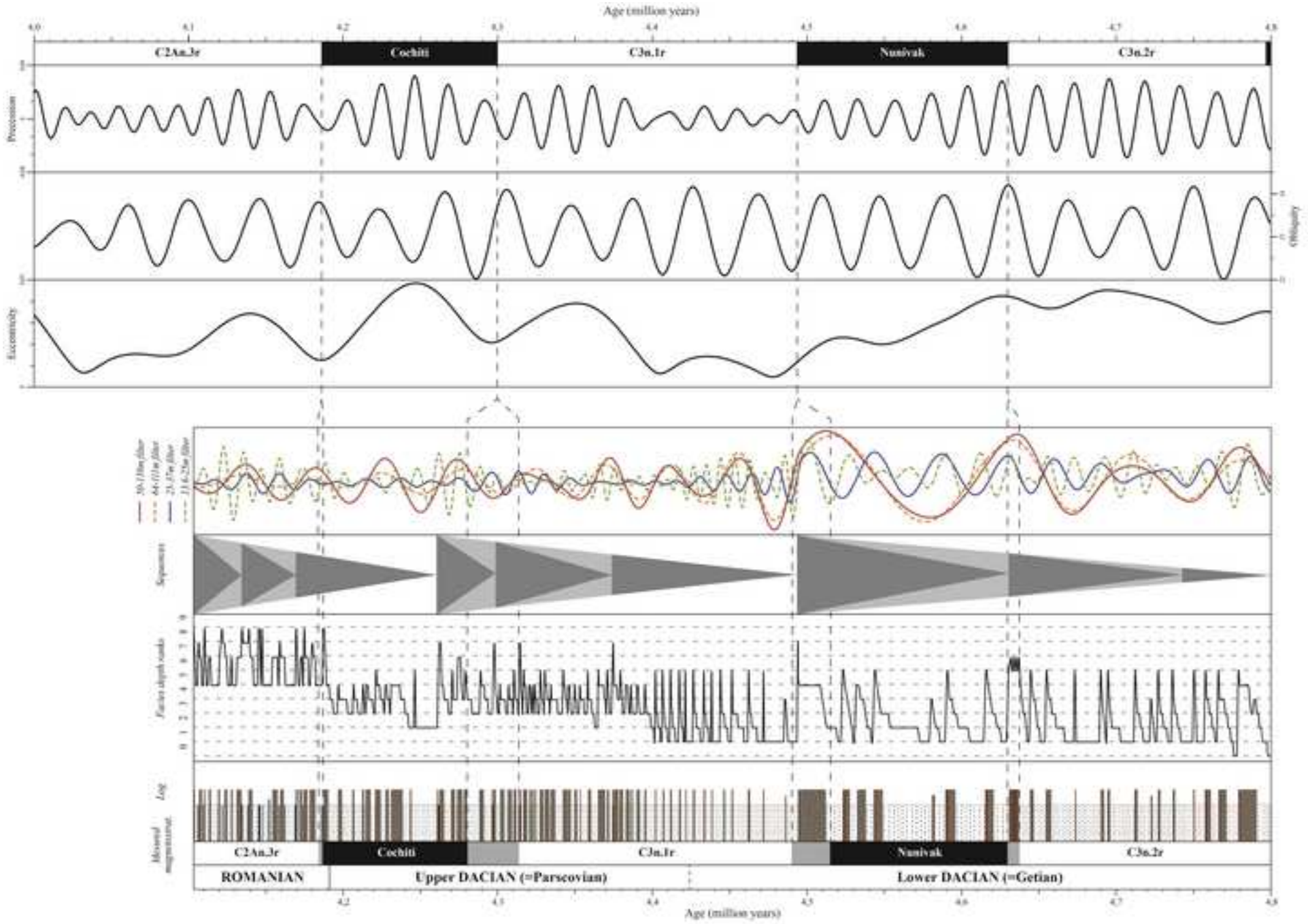

Figure 18

Click here to download high resolution image

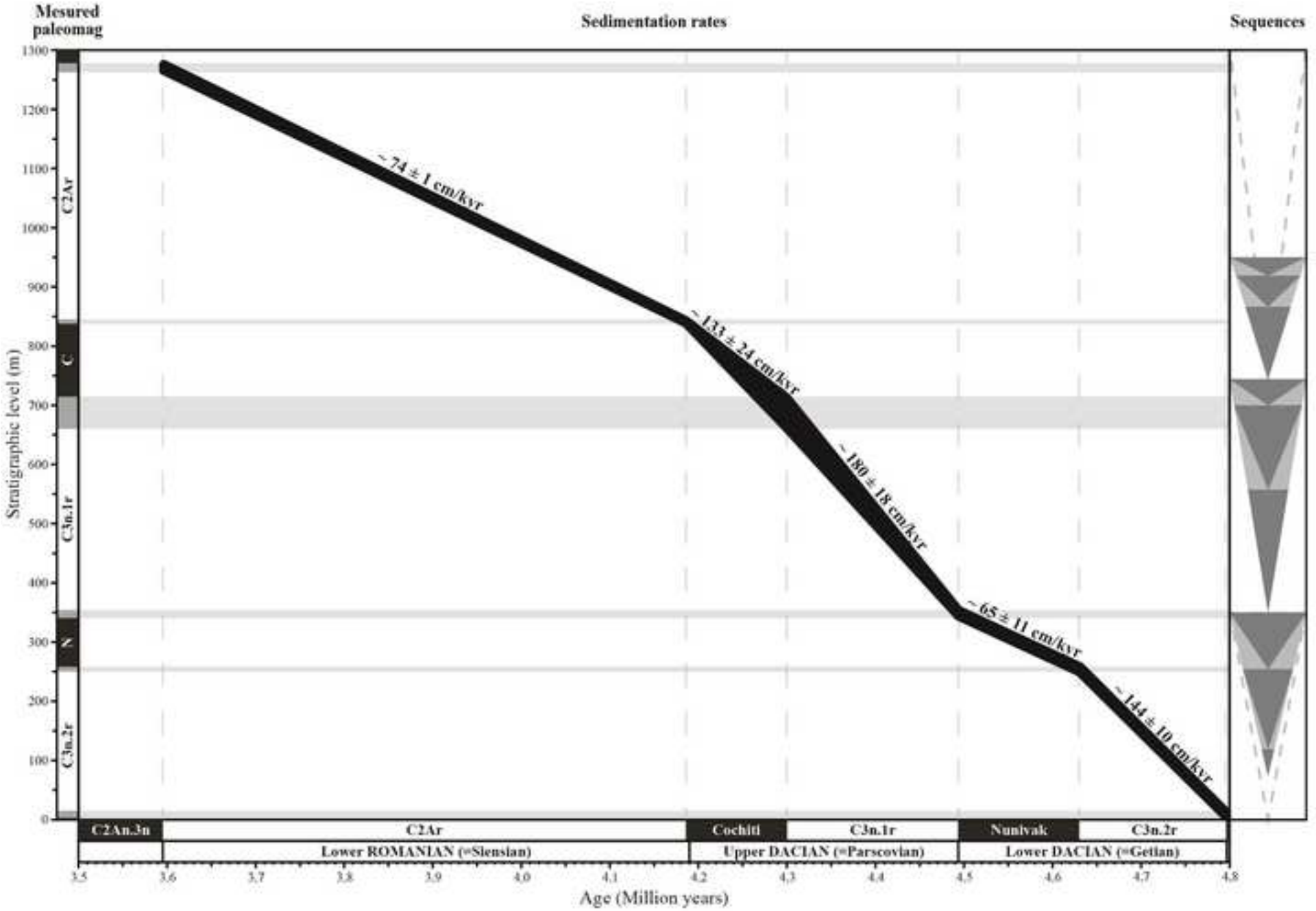

Table 1

Click here to download high resolution image

Index	Depositional environment	Sedimentary structures
0	Shelf	Structureless mudstones, *in situ* brackish-water fauna
1	Distal pro-delta	Mudstones with millimeter-scale planar laminations of silts
2	Proximal pro-delta	Mudstones with centimeter-scale lenticular bedding of silts and very-fine-grained sandstones
3	Distal delta-front	Mudstones with centimeter-scale cross-bedding of very-fine-grained sandstones
4	Proximal delta-front	Mudstones with decimeter-scale cross-bedding of very-fine-grained sandstones
5	Distributary mouth bar/Interdistributary bay	Medium-grained sandstones with decimeter to meter-scale cross-bedding, erosive base, reworked fresh-water fauna
6	Flooding surface	Medium to coarse-grained sandstones, erosive base, reworked glauconite, reworked brackish- and fresh-water fauna
7	Channel fill	Fine-grained sandstones, centimeter-scale cross-bedding, organic material fragments
8	Coastal-plain mire	Structureless clays, enrichment in organic material, *in situ* fresh-water fauna, burrows
9	Peat	Structureless clays, coal layers, roots

Table 2

Click here to download high resolution image

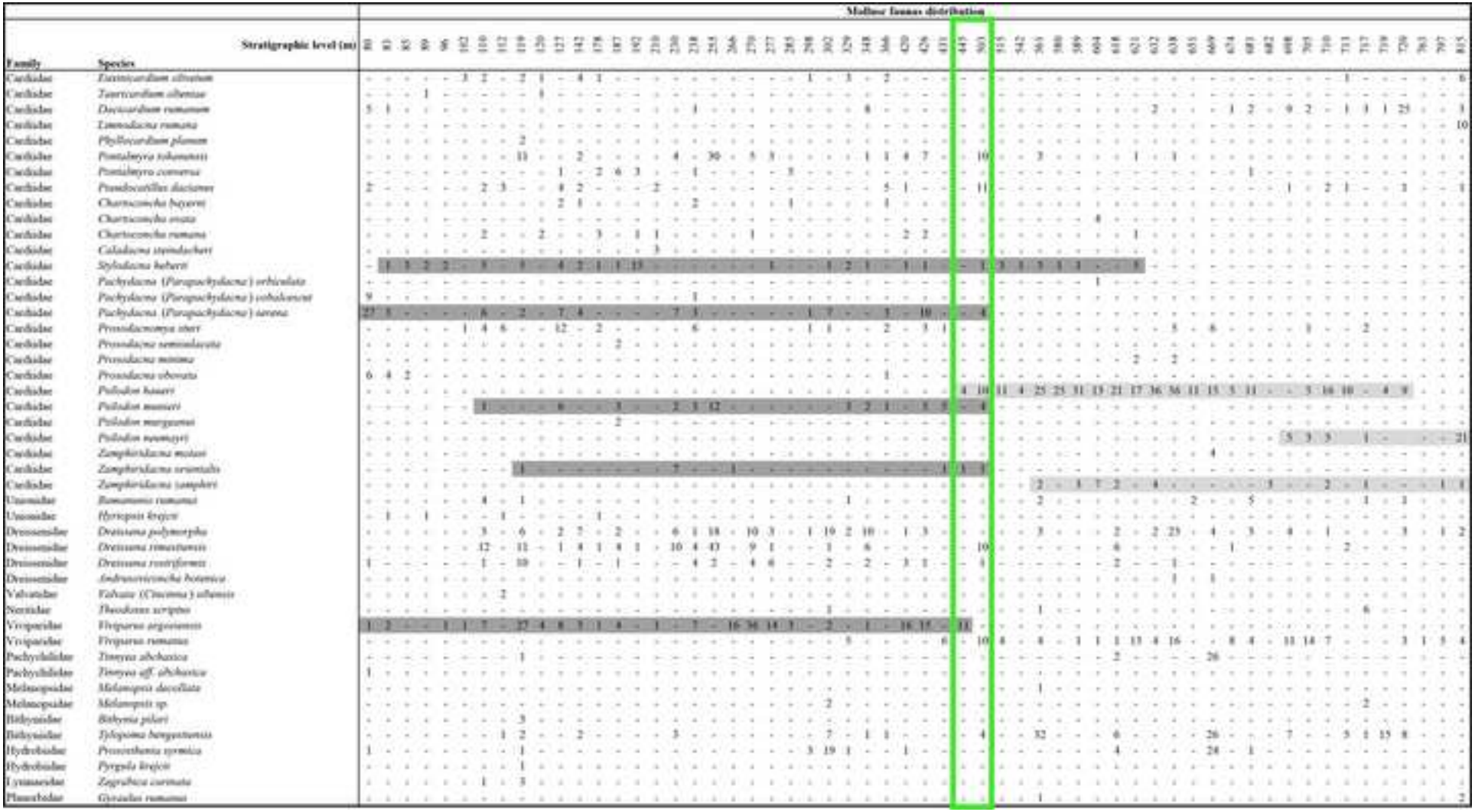

Table 3

Click here to download high resolution image

Code	Lithofacies	Grain size	Sedimentary structures	Inclusions	Processes	Fig.
Sfr	Reddish shell-rich sandstone	Fine to medium	Erosive base, indurated, reddish oxidation, hints of low-angle cross-stratification	Reworked brackish and fresh-water molluscs, glauconite	Very high energy flow, sediment reworking, winnowing, post-depositional diagenic induration	11f
Sfg	Greyish shell-rich sandstone	Fine to medium	Structureless, indurated	Reworked brackish and fresh-water molluscs, ichnofossils	Very high energy flow, sediment reworking, post-depositional diagenic induration	11e
St	Trough cross-stratified sandstone	Very fine to medium	Trough cross-stratification, preserved cross-set thickness of 10-50cm, unidirectional	Organic fragments along foresets	Moderate energy flow, migration of sinous crested dunes	11d
Ss	Sigmoidal cross-stratified sandstone	Fine to medium	Sigmoidal cross-stratification, preserved cross-set thickness of 20-100cm, unidirectional	Organic fragments along foresets	Moderate to high energy flow, migration of straight crested dunes	11c
Sr	Climbing rippled sandstone	Very fine to medium	Climbing ripples, preserved cross-set thickness of 10-50cm, unidirectional	Organic fragments along foresets	Moderate energy flow, migration of curved crested ripples, abundant suspended material	11b
Sc	Current rippled sandstone	Fine to medium	Asymmetrical current ripples, amplitude of 3-5cm, wavelenght of 7-10cm	Organic fragments along foresets	Moderate energy, migration of ripples, abundant suspended material	11a
Sh	Horizontally laminated sandstone	Fine to medium	Horizontal laminations, possible normal and inverse grading, possible erosive base	Laminations with possible organic fragments	Low or high energy, plane-bed flow	10g
Sl	Low-angle cross-stratified sandstone	Fine to medium	Low-angle cross-stratification, preserved cross-set thickness of 30-200cm, unidirectional	Organic fragments along foresets	High energy flow, migration of low relief dunes	10f
Sm	Massive sandstone	Fine to medium	Structureless, inverse grading, dm-scale troughs filled in with organic debris	Reworked fresh-water molluscs, ichnofossils	Low energy flow	10e
Fs	Lenticular mudstone	Mudstone	Cm-scale lenticular bedding of trough cross-stratified very fine sand, preserved cross-set thickness of 1-5cm, unidirectional	Organic fragments along foresets	Fluctuations between very low and moderate energy, deposition from suspension and distal outflows	10d
Fl	Laminated mudstone	Mudstone	Mm-scale planar laminations	Laminations with silt and organic fragments	Fluctuations between very low and moderate energy, deposition from suspension and distal outflows	10c
Fm	Massive mudstone	Mudstone	Structureless	*In situ* brackish-water molluscs	Very low energy, deposition from suspension	10b
C	Organic-rich clay	Clay	Structureless, possible coal layers, possible induration	*In situ* fresh-water molluscs, ichnofossils, roots, organic fragments	Very low energy, deposition from suspension, sometimes subaerially exposured	10a

Table 4

Click here to download high resolution image